RDECOM TR 10-D-111

**U.S. ARMY RESEARCH,
DEVELOPMENT AND
ENGINEERING COMMAND**

TITLE:	**Design and Experimental Results for the S411 Airfoil**
AUTHOR:	**Dan M. Somers and Mark D. Maughmer**
COMPANY NAME:	**Airfoils, Incorporated**
COMPANY ADDRESS:	**122 Rose Drive** **Port Matilda PA 16870-7535**
DATE:	**August 2010**
FINAL REPORT:	**Contract Number W911W6-07-C-0047, SBIR Phase II,** **Topic Number A06-006, Proposal Number A2-2972**

Prepared for:

**U.S. ARMY RESEARCH, DEVELOPMENT AND ENGINEERING COMMAND,
AVIATION APPLIED TECHNOLOGY DIRECTORATE, FORT EUSTIS, VA 23604-5577**

DESIGN AND EXPERIMENTAL RESULTS FOR THE S411 AIRFOIL

DAN M. SOMERS
AIRFOILS, INCORPORATED

MARK D. MAUGHMER
THE PENNSYLVANIA STATE UNIVERSITY

AUGUST 2010

ABSTRACT

A 14-percent-thick airfoil, the S411, intended for rotorcraft applications has been designed and analyzed theoretically and verified experimentally in The Pennsylvania State University Low-Speed, Low-Turbulence Wind Tunnel. The airfoil incorporates a 5-percent-chord tab. The two primary objectives of high maximum lift and low profile drag have been achieved. The constraint on the pitching moment has been exceeded; that on the airfoil thickness, satisfied. The airfoil exhibits a docile stall. Comparisons of the theoretical and experimental results generally show good agreement. Comparisons with the S406 airfoil confirm the achievement of the objectives.

INTRODUCTION

Almost all airfoils in use on rotorcraft today were developed under the assumption that extensive laminar flow is not likely on a rotor. (See ref. 1, for example.) For the present application, however, given the relatively low Reynolds numbers and the precision blade manufacturing technique being employed, the achievement of laminar flow warrants exploration.

The airfoil designed under the present effort is intended for the rotor of a small helicopter. To complement the design effort, an investigation was conducted in The Pennsylvania State University Low-Speed, Low-Turbulence Wind Tunnel (ref. 2) to obtain the basic, low-speed, two-dimensional aerodynamic characteristics of the airfoil. The results have been compared with predictions from the method of references 3 and 4 and from the method of reference 5. The results have also been compared with those for the S406 airfoil (ref. 6), which has similar design specifications.

SYMBOLS

Values are given in both SI and U.S. Customary Units. Measurements and calculations were made in U.S. Customary Units.

C_p pressure coefficient, $\dfrac{p_l - p_\infty}{q_\infty}$

c airfoil chord, mm (in.)

c_c section chord-force coefficient, $\oint C_p \, d\left(\dfrac{z}{c}\right)$

c_d section profile-drag coefficient, $\displaystyle\int_{\text{Wake}} c_d' \, d\left(\dfrac{h}{c}\right)$, except post stall, $c_n \sin\alpha + c_c \cos\alpha$

c_d' point drag coefficient (ref. 7)

c_l section lift coefficient, $c_n / \cos\alpha - c_d \tan\alpha$

c_m section pitching-moment coefficient about quarter-chord point,

$$-\oint C_p\left(\frac{x}{c} - 0.25\right) d\left(\frac{x}{c}\right) + \oint C_p\left(\frac{z}{c}\right) d\left(\frac{z}{c}\right)$$

c_n section normal-force coefficient, $-\oint C_p d\left(\frac{x}{c}\right)$

h   horizontal width in wake profile, mm (in.)

M   free-stream Mach number

p   static pressure, Pa (lbf/ft^2)

q   dynamic pressure, Pa (lbf/ft^2)

R   Reynolds number based on free-stream conditions and airfoil chord

t   airfoil thickness, mm (in.)

x   airfoil abscissa, mm (in.)

y   model span station, $y = 0$ at midspan, mm (in.)

z   airfoil ordinate, mm (in.)

α angle of attack relative to x-axis, deg

Subscripts:

l local point on airfoil

ll   lower limit of low-drag range

max   maximum

min   minimum

S   separation

T   transition

ul   upper limit of low-drag range

0   zero lift

∞ free-stream conditions

2

Abbreviations:

L.   lower surface

S.   boundary-layer separation location, x_S/c

T.   boundary-layer transition location, x_T/c

U.   upper surface

AIRFOIL DESIGN

OBJECTIVES AND CONSTRAINTS

The airfoil design specifications are contained in table I. Two primary objectives are evident. The first objective is to achieve a maximum lift coefficient of 1.25 at a Mach number of 0.30 and a Reynolds number of 0.97×10^6 and a maximum lift coefficient of 1.20 at a Mach number of 0.40 and a Reynolds number of 1.29×10^6. A requirement related to this objective is that the maximum lift coefficient not decrease significantly with transition fixed near the leading edge on both surfaces. In addition, the airfoil should exhibit docile stall characteristics. The second objective is to obtain low profile-drag coefficients from a lift coefficient of 0.10 at a Mach number of 0.70 and a Reynolds number of 2.26×10^6 to a lift coefficient of 0.65 at a Mach number of 0.45 and a Reynolds number of 1.45×10^6.

Three major constraints were placed on the design of the airfoil. First, the zero-lift pitching-moment coefficient must be 0 ± 0.002 at a Mach number of 0.75 and a Reynolds number of 2.42×10^6 with transition fixed at 10-percent chord on the upper and lower surfaces and 0 ± 0.005 at a Mach number of 0.45 and a Reynolds number of 1.45×10^6 with transition free. Second, the airfoil must incorporate a tab having a length of 5-percent chord and a thickness of 0.352-percent chord. Third, the airfoil thickness must equal 14-percent chord with the tab.

The specifications for this airfoil are similar to those for the S406 airfoil (ref. 6), except the pitching-moment constraint is tighter.

PHILOSOPHY

Given the above objectives and constraints, certain characteristics of the design are apparent. The following sketch illustrates a drag polar that meets the goals for this design.
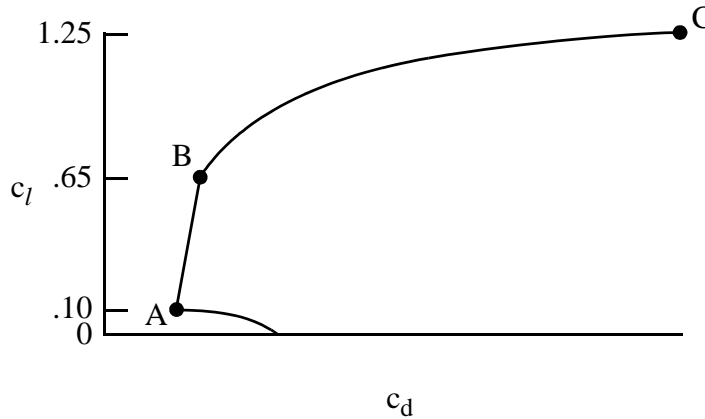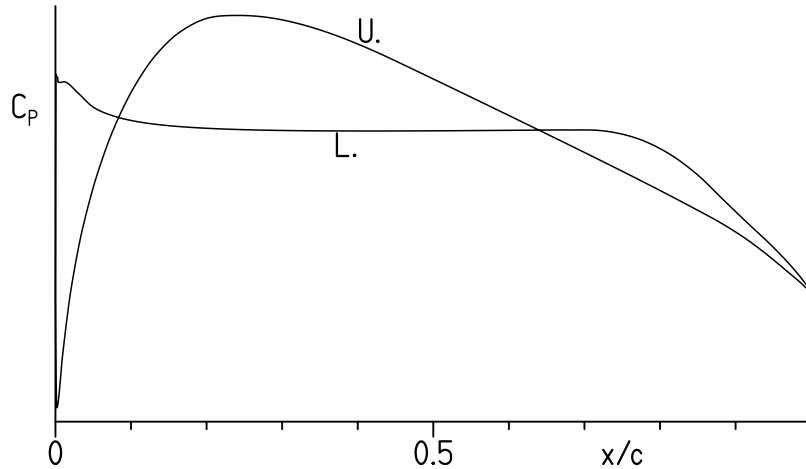

Sketch 1

The desired airfoil shape can be traced to the pressure distributions that occur at the various points in sketch 1. Point A is the lower limit of the low-drag range of lift coefficients; point B, the upper limit. The profile-drag coefficient at point B is not as low as at point A, unlike the polars of many laminar-flow airfoils where the drag coefficient within the laminar bucket is nearly constant. (See, for example, ref. 8.) This characteristic is related to the elimination of significant (i.e., drag-producing) laminar separation bubbles on the upper surface for the design range of Reynolds numbers. (See ref. 9.) The drag coefficient increases rapidly outside the low-drag, lift-coefficient range because boundary-layer transition moves quickly toward the leading edge with increasing (or decreasing) lift coefficient. This feature results in a leading edge that produces a suction peak at higher lift coefficients, which ensures that transition on the upper surface will occur very near the leading edge. Thus, the maximum lift coefficient, point C, occurs with turbulent flow along the entire upper surface and, therefore, should be relatively insensitive to roughness at the leading edge.

An unusual design approach was taken for this airfoil. Rather than design a thicker airfoil and then add the required tab, the airfoil was designed from the outset for the specified thickness including the tab. Specifically, the airfoil was initially designed with a trailing-edge shape that geometrically and aerodynamically approximated the tab. This shape was then modified to the required tab geometry. Accordingly, the performance of the final, tabbed airfoil is likely better than that of an airfoil altered by the addition of a relatively arbitrary tab.

4

From the preceding discussion, the pressure distributions along the polar can be deduced. The pressure distribution at point A for the airfoil shape with the pseudo tab should look something like sketch 2.

Sketch 2

To achieve low drag, a favorable pressure gradient is desirable along the upper surface to about 25-percent chord. Aft of this point, a short region having a shallow, adverse pressure gradient (i.e., a "transition ramp") promotes the efficient transition from laminar to turbulent flow (ref. 10). The transition ramp is followed by a very slightly convex pressure recovery. The specific pressure recovery employed represents a compromise between maximum lift, drag, pitching moment, stall characteristics, and drag divergence. The steeper, adverse pressure gradient aft of about 90-percent chord is a "separation ramp," originally proposed by F. X. Wortmann,[1] which confines turbulent separation to a small region near the trailing edge. By constraining the movement of the separation point at high angles of attack, higher lift coefficients can be achieved with little drag penalty. This feature has the added benefit of promoting docile stall characteristics. (See ref. 11.)

Along the lower surface, the pressure gradient is initially adverse, then zero, and then favorable to about 70-percent chord. Thus, transition is imminent over the entire forward portion of the lower surface. (See ref. 12.) This concept allows a wide low-drag range to be achieved and increases the loading in the leading-edge region. The forward loading serves to balance, with respect to the pitching-moment constraint, the aft loading, both of which contribute to the achievement of the specified maximum lift coefficient and low profile-drag coefficients. This region is followed by a transition ramp and then a roughly linear pressure recovery. The pressure recovery must begin farther forward than optimum for low drag and

---

[1]Director, Institute for Aerodynamics and Gas Dynamics, University of Stuttgart, Germany, 1974–1985.

the constrained pitching moment to alleviate separation at lower lift coefficients, especially with transition fixed near the leading edge.

The amounts of pressure recovery on the upper and lower surfaces are determined by the airfoil-thickness and pitching-moment constraints.

At point B, the pressure distribution should look like sketch 3.
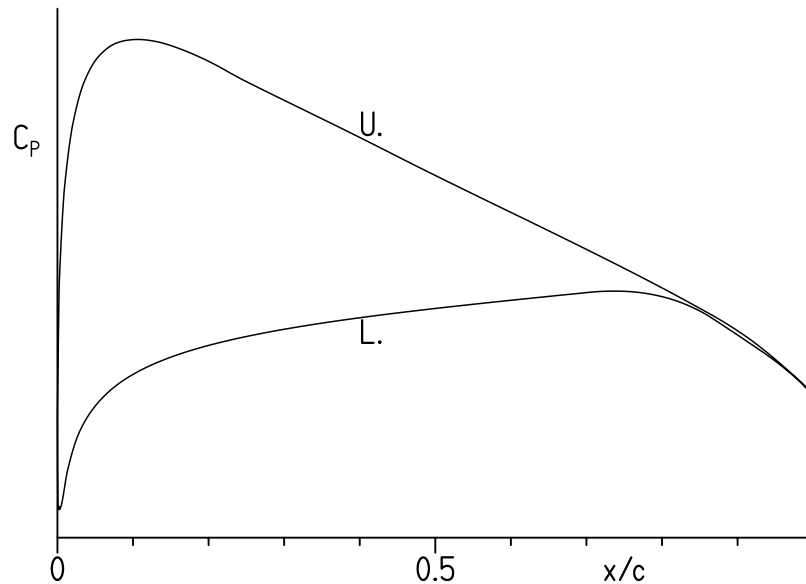
Sketch 3

No suction peak exists at the leading edge. Instead, a rounded peak occurs aft of the leading edge, which allows some laminar flow, although not to the extent of point A.

EXECUTION

Given the pressure distributions previously discussed, the design of the airfoil is reduced to the inverse problem of transforming the pressure distributions into an airfoil shape. The Eppler Airfoil Design and Analysis Code (refs. 3 and 4) was used because of its unique capability for multipoint design and because of confidence gained during the design, analysis, and experimental verification of many other airfoils. (See ref. 13, for example.) The code also offers useful options for the modification of the airfoil geometry with respect to the tab.

The airfoil is designated the S411. The airfoil shape incorporates a tab that is 5-percent-chord long and 0.352-percent-chord thick, which satisfies the design constraint.

The airfoil shape and coordinates are available from Airfoils, Incorporated. The airfoil thickness is 14.00-percent chord, which satisfies the design constraint.

THEORETICAL PROCEDURE

The theoretical results are predicted using the method of references 3 and 4 (PROFIL07), commonly known as the Eppler code, and the method of reference 5 (MSES 3.0). Critical amplification factors of 11 and 9 were specified for the computations using the method of references 3 and 4 and the method of reference 5, respectively. Because the maximum lift coefficient computed by the method of references 3 and 4 is not always realistic, an empirical criterion has been applied to the computed results. The criterion assumes the maximum lift coefficient has been reached if the drag coefficient of the upper surface reaches a certain value that is a function of the Reynolds number and the wind-tunnel facility. It should also be noted that the compressibility correction (ref. 14) incorporated in the method of references 3 and 4 is invalid if the local flow is supersonic.

Because the free-stream Mach number for all wind-tunnel test conditions did not exceed 0.2, the flow can be considered essentially incompressible for the purpose of comparing the theoretical and experimental results. This allows the fast, subcritical flow solver of the method of reference 5 to be used.

EXPERIMENTAL PROCEDURE

WIND TUNNEL

The Pennsylvania State University Low-Speed, Low-Turbulence Wind Tunnel (ref. 2) is a closed-throat, single-return, atmospheric tunnel (fig. 1). The test section is 101.3 cm (39.9 in.) high by 147.6 cm (58.1 in.) wide (fig. 2). Electrically actuated turntables provide positioning and attachment for the two-dimensional model. The turntables are flush with the top and bottom tunnel walls and rotate with the model. The axis of rotation coincided approximately with the midchord of the model, which was mounted vertically between the turntables. The gaps between the model and the turntables were sealed. The turbulence intensity in the test section is approximately 0.05 percent at 46 m/s (150 ft/s).

MODEL

The aluminum, wind-tunnel model was fabricated by Skytop Aerospace, Bellefonte, Pennsylvania, using a numerically controlled milling machine. The model had a chord of 457.2 mm (18.00 in.) and a span of 107.95 cm (42.50 in.) and, thus, extended through both turntables. Upper- and lower-surface orifices were located to one side of midspan at the staggered positions listed in table II. All the orifices were 0.51 mm (0.020 in.) in diameter with their axes perpendicular to the surface. The surfaces of the model were sanded to ensure an

aerodynamically smooth finish. The measured model contour was within 0.13 mm (0.005 in.) of the prescribed shape.

WAKE-SURVEY PROBE

A total- and static-pressure, wake-survey probe (fig. 3) was mounted from the top tunnel wall (fig. 2). The probe was positioned at midspan and automatically aligned with the wake-centerline streamline. A traverse mechanism incrementally positioned the probe to survey the wake. The increment was 1.27 mm (0.050 in.) for traverses less than 254.0 mm (10.00 in.) and 2.54 mm (0.100 in.) for longer traverses, which were occasionally required near the maximum lift coefficient. The tip of the probe was located 0.83 chord downstream of the trailing edge of the model.

INSTRUMENTATION

Basic tunnel pressures and the wake pressures were measured with precision transducers. Measurements of the pressures on the model were made by an automatic pressure-scanning system utilizing precision transducers. Data were obtained and recorded by an electronic data-acquisition system.

METHODS

The pressures measured on the model were reduced to standard pressure coefficients and numerically integrated to obtain section normal-force and chord-force coefficients and section pitching-moment coefficients about the quarter-chord point. Section profile-drag coefficients were computed from the wake total and static pressures by the method of reference 7. Wake surveys were not performed, however, at most post-stall angles of attack, in which case, the profile-drag coefficients were computed from the normal- and chord-force coefficients.

Standard, low-speed, wind-tunnel boundary corrections (ref. 15) have been applied to the data. It should be noted, however, that the pressure distributions themselves are uncorrected. The wake-survey-probe total-pressure-tube displacement correction (ref. 7) has been taken into account.

TESTS

The model was tested at Reynolds numbers based on airfoil chord of 0.5×10^6, 0.7×10^6, 1.0×10^6, and 1.5×10^6 with transition free (smooth), with transition fixed by roughness at 10-percent chord on the upper and lower surfaces to simulate a possible manufacturing deficiency, and with transition fixed by roughness near the leading edge, 2-percent chord on the upper surface and 7-percent chord on the lower surface, to simulate full-chord,

turbulent flow. Using the method of reference 16, the grit roughness was sized for lower lift coefficients for the 10-percent-chord location and for higher lift coefficients for the locations near the leading edge. The grit was sparsely distributed along 3-mm (0.1-in.) wide strips applied to the model with lacquer. (See table III.) The Mach number did not exceed 0.2 for any test condition.

It should be noted that the test Mach numbers are much lower than the operational values of the intended application.

Starting from 0°, the angle of attack was increased to post-stall values. The angle of attack was then decreased from 0° to below that for zero lift.

DISCUSSION OF RESULTS

THEORETICAL RESULTS

Pressure Distributions

The inviscid pressure distributions at various angles of attack at Mach numbers of 0.30 and 0.45 predicted using the method of references 3 and 4 are shown in figure 4. The (viscous) pressure distributions at various angles of attack at a Mach number of 0.70 and a Reynolds number of 2.26×10^6 predicted using the method of reference 5 are shown in figure 5.

Section Characteristics

The section characteristics at three of the design conditions with transition free and transition fixed are shown in figures 6 through 8. Based on the predictions, all the design objectives and constraints have been met, except for the zero-lift pitching-moment coefficient, which exceeds the constraint.

EXPERIMENTAL RESULTS

Pressure Distributions

The pressure distributions at various angles of attack for a Reynolds number of 1.00×10^6 and a Mach number of 0.10 with transition free are shown in figure 9. At an angle of attack of −2.01° (fig. 9(a)), transition probably occurs around 60-percent chord on the upper surface and near the leading edge on the lower surface. At an angle of attack of −1.00° (fig. 9(a)), which corresponds approximately to the lower limit of the low-drag, lift-coefficient range, a short laminar separation bubble is evident on the lower surface around 85-percent chord. As the angle of attack is increased, a short laminar separation bubble becomes more evident on the upper surface and moves forward, whereas the bubble on the lower surface remains relatively fixed (figs. 9(a)–9(c)). At an angle of attack of 8.16° (fig. 9(c)), turbulent,

trailing-edge separation occurs on the upper surface. The amount of separation increases with increasing angle of attack (figs. 9(c) and 9(d)). The maximum lift coefficient occurs between the angles of attack of 12° and 13° (figs. 9(c) and 9(d)). As the angle of attack is increased further, the separation point continues to move forward, although the leading-edge pressure peak does not fall (fig. 9(d)).

Section Characteristics

The section characteristics with transition free and transition fixed are shown in figure 10 and tabulated in the appendix. For a Reynolds number of 1.00×10^6 and a Mach number of 0.10 with transition free (fig. 10(c)), the maximum lift coefficient is 1.26. For a Reynolds number of 1.50×10^6 and a Mach number of 0.16 with transition free (fig. 10(d)), the lower limit of the low-drag range of lift coefficients is approximately 0.05, the maximum lift-to-drag ratio occurs at a lift coefficient of about 0.96, and the zero-lift pitching-moment coefficient is −0.001. (Because the upper limit of the low-drag, lift-coefficient range is not sharply defined, a precise value for the upper limit cannot be given.)

The effects of Reynolds number on the section characteristics are summarized in figure 11. In general, with transition free, the lift-curve slope, the maximum lift coefficient, and the lower limit of the low-drag range increase with increasing Reynolds number. The zero-lift angle of attack, the profile-drag coefficients, and the pitching-moment coefficients, including the zero-lift value, generally decrease with increasing Reynolds number. The airfoil exhibits docile stall characteristics that become less docile with increasing Reynolds number.

The effect of fixing transition on the section characteristics is shown in figure 10. In general, the zero-lift angle of attack, the lift-curve slope, the maximum lift coefficient, and the pitching-moment coefficients, including the zero-lift value, decrease with transition fixed. These results are primarily a consequence of the boundary-layer displacement effect, which decambers the airfoil because the displacement thickness is greater with transition fixed than with transition free. In addition, the maximum lift coefficient decreases with transition fixed because the roughness induces earlier trailing-edge separation. Accordingly, the decrease in maximum lift coefficient is inversely proportional to the roughness location, averaging 1 percent over the test Reynolds number range with transition fixed at 10-percent chord on the upper and lower surfaces and 9 percent with transition fixed at 2-percent chord on the upper surface and 7-percent chord on the lower surface. The elimination of the laminar separation bubble on the lower surface (see fig. 9) by the roughness also contributes to the decrease in the pitching-moment coefficient. The drag coefficients are, of course, generally affected adversely by the roughness. The stall characteristics are less docile with transition fixed.

It should be noted that, for most test conditions, the Reynolds number based on local velocity and boundary-layer displacement thickness at the forward roughness locations, 2-percent and 7-percent chord, is too low to support turbulent flow. (See ref. 17.) Accordingly, to force transition, the roughness must be so large that it increases the displacement thickness, which abnormally decreases the lift coefficient and the magnitude of the pitching-moment coefficient and increases the drag coefficient. Conversely, at low lift coefficients, the

roughness on the upper surface, which is sized for higher lift coefficients, is too small to force transition, resulting in incorrectly low drag coefficients. For Reynolds numbers of 0.50×10^6 and 0.70×10^6 (figs. 10(a) and 10(b)), the roughness near the leading edge alleviates the laminar separation bubble on the lower surface, thereby actually decreasing the drag coefficient.

The variations of maximum lift coefficient and minimum profile-drag coefficient with Reynolds number are shown in figures 12 and 13, respectively. With transition free, the maximum lift coefficient increases with increasing Reynolds number, whereas the minimum profile-drag coefficient decreases, which are typical trends for most airfoils. (The minimum drag coefficient with transition fixed at 2-percent chord on the upper surface and 7-percent chord on the lower surface is too low because the roughness is too small to force transition at lower lift coefficients, as previously discussed.)

COMPARISON OF THEORETICAL AND EXPERIMENTAL RESULTS

Pressure Distributions

The comparison of the theoretical and experimental pressure distributions at various angles of attack is shown in figure 14. It should be noted that the pressure distributions predicted using the method of references 3 and 4 (PROFIL07) are inviscid and incompressible, whereas the pressure distributions predicted using the method of reference 5 (MSES 3.0) as well as the experimental pressure distributions were obtained for a Reynolds number of 1.00×10^6 and a Mach number of 0.10 with transition free. It should also be noted that the theoretical lift coefficient from the method of references 3 and 4 is calculated from the lift-curve slope and the angle of attack relative to the zero-lift line, whereas the lift coefficient from the method of reference 5 and from the experiment is derived from the integrated pressure distribution. (See refs. 3–5 and 7.) Thus, at a given lift coefficient, the pressure distribution predicted using the method of references 3 and 4 does not necessarily have the same area as the measured pressure distribution. It should be noticed that the angle of attack shown in figure 14 is the theoretical value from the method of references 3 and 4, not the experimental value. Also, the lift coefficient shown in this figure only is the uncorrected value.

With respect to the method of references 3 and 4, at a lift coefficient of 0.13 (fig. 14(a)), which is near the lower limit of the low-drag range, the pressure coefficients and the pressure gradients agree well, except where laminar separation bubbles are present and along the upper surface in the vicinity of the start of the tab. The latter disparity is probably the result of the displacement effect. At a lift coefficient of 0.61 (fig. 14(b)), although the pressure coefficients do not match exactly, the pressure gradients agree reasonably well, again except where bubbles are present and along the upper surface near the start of the tab. At a lift coefficient of 1.14 (fig. 14(c)), which is near the experimental maximum lift coefficient, the agreement is poor because the effect of the upper-surface, trailing-edge separation on the pressure distribution is not modelled in the method of references 3 and 4.

With respect to the method of reference 5, at a lift coefficient of 0.13 (fig. 14(a)), the pressure coefficients and the pressure gradients agree remarkably well. The location of the

lower-surface laminar separation bubble is predicted well, but that of the upper-surface bubble is aft of the measured location. At a lift coefficient of 0.61 (fig. 14(b)), although the pressure coefficients do not match exactly, the pressure gradients agree well. The predicted location of the upper-surface bubble is again aft of the measured location. At a lift coefficient of 1.14 (fig. 14(c)), the agreement is less exact because the extent of the upper-surface, trailing-edge separation and, in turn, its effect on the overall circulation are underpredicted by the method of reference 5.

Section Characteristics

The comparison of the theoretical and experimental section characteristics with transition free is shown in figure 15. The previously discussed empirical criterion applied to the results from the method of references 3 and 4 (PROFIL07) underestimates the maximum lift coefficient by an average of 11 percent over the test Reynolds number range. The method of reference 5 (MSES 3.0) overpredicts the maximum lift coefficient by an average of 17 percent. The method of references 3 and 4 generally overpredicts the profile-drag coefficients, whereas the method of reference 5 generally underpredicts the drag coefficients. Both methods predict the zero-lift angle of attack, the lift-curve slope, the lower limit of the low-drag range, and the zero-lift pitching-moment coefficient reasonably well. Both methods also predict more positive pitching-moment coefficients and underpredict the effect of the trailing-edge separation on the lift coefficient at higher angles of attack. Overall, the general agreement improves with increasing Reynolds number.

The comparison of the theoretical and experimental section characteristics with transition fixed at 10-percent chord on the upper and lower surfaces is shown in figure 16. In general, the predicted characteristics show similar tendencies as with transition free. The method of references 3 and 4 underpredicts the magnitude of the pitching-moment coefficients at lower angles of attack, whereas the method of reference 5 predicts the values well.

The comparison of the theoretical and experimental section characteristics with transition fixed at 2-percent chord on the upper surface and 7-percent chord on the lower surface is shown in figure 17. In general, the predicted characteristics show similar tendencies as with transition free, although the general agreement is poorer, particularly with respect to the drag coefficients, probably because of the abnormalities introduced by the roughness, as discussed previously. The empirical criterion applied to the results from the method of references 3 and 4 underpredicts the maximum lift coefficient by an average of 6 percent, whereas the method of reference 5 overpredicts the maximum lift coefficient by an average of 28 percent. The method of reference 5 overpredicts the magnitude of the pitching-moment coefficients at lower angles of attack, whereas the method of references 3 and 4 predicts the values well.

Given the abrupt, contour changes introduced by the tab, the agreement between the theoretical and experimental section characteristics is remarkably good overall.

COMPARISON WITH S406 AIRFOIL

The section characteristics of the S411 airfoil for a Reynolds number of 1.00×10^6 and a Mach number of 0.10 with transition free are compared with those of the S406 airfoil, which has similar design specifications, in figure 18. The maximum lift coefficients and the profile-drag coefficients at a lift coefficient of 0.4 are compared in figures 19 and 20, respectively. The maximum lift coefficients with transition free are nearly identical, but the S411 airfoil suffers a larger effect of roughness. The S411 airfoil exhibits substantially higher drag coefficients but also substantially less negative pitching-moment coefficients.

CONCLUDING REMARKS

A 14.00-percent-thick airfoil, the S411, intended for rotorcraft applications has been designed and analyzed theoretically and verified experimentally in The Pennsylvania State University Low-Speed, Low-Turbulence Wind Tunnel. The airfoil incorporates a 5-percent-chord tab. The two primary objectives of a high maximum lift coefficient and low profile-drag coefficients have been achieved. The constraint on the zero-lift pitching-moment coefficient has been exceeded; the constraint on the airfoil thickness has been satisfied. The airfoil exhibits docile stall characteristics. Comparisons of the theoretical and experimental results generally show good agreement. Comparisons with the S406 airfoil confirm the achievement of the objectives.

ACKNOWLEDGMENTS

REFERENCES

1. Noonan, Kevin W.: Aerodynamic Characteristics of Two Rotorcraft Airfoils Designed for Application to the Inboard Region of a Main Rotor Blade. NASA TP-3009, 1990.

2. Brophy, Christopher M.: Turbulence Management and Flow Qualification of The Pennsylvania State University Low Turbulence, Low Speed, Closed Circuit Wind Tunnel. M. S. Thesis, Pennsylvania State Univ., 1993.

3. Eppler, Richard: Airfoil Design and Data. Springer-Verlag (Berlin), 1990.

4. Eppler, Richard: Airfoil Program System "PROFIL07." User's Guide. Richard Eppler, c.2007.

5. Drela, M.: Design and Optimization Method for Multi-Element Airfoils. AIAA Paper 93-0969, Feb. 1993.

6. Somers, Dan M.; and Maughmer, Mark D.: Design and Experimental Results for the S406 Airfoil. U.S. Army RDECOM TR 10-D-107, 2010. (Available from DTIC.)

7. Pankhurst, R. C.; and Holder, D. W.: Wind-Tunnel Technique. Sir Isaac Pitman & Sons, Ltd. (London), 1965.

8. Abbott, Ira H.; Von Doenhoff, Albert E.; and Stivers, Louis S., Jr.: Summary of Airfoil Data. NACA Rep. 824, 1945. (Supersedes NACA WR L-560.)

9. Eppler, Richard; and Somers, Dan M.: Airfoil Design for Reynolds Numbers Between 50,000 and 500,000. Proceedings of the Conference on Low Reynolds Number Airfoil Aerodynamics, UNDAS-CP-77B123, Univ. of Notre Dame, June 1985, pp. 1–14.

10. Wortmann, F. X.: Experimental Investigations on New Laminar Profiles for Gliders and Helicopters. TIL/T.4906, British Minist. Aviat., Mar. 1960. (Translated from Z. Flugwissenschaften, Bd. 5, Heft 8, Aug. 1957, S. 228–243.)

11. Maughmer, Mark D.; and Somers, Dan M.: Design and Experimental Results for a High-Altitude, Long-Endurance Airfoil. J. Aircr., vol. 26, no. 2, Feb. 1989, pp. 148–153.

12. Eppler, R.: Laminar Airfoils for Reynolds Numbers Greater Than 4×10^6. B-819-35, Apr. 1969. (Available from NTIS as N69-28178; translated from Ingenieur-Archiv, Bd. 38, Heft 4/5, 1969, S. 232–240.)

13. Somers, Dan M.: Subsonic Natural-Laminar-Flow Airfoils. Natural Laminar Flow and Laminar Flow Control, R. W. Barnwell and M. Y. Hussaini, eds., Springer-Verlag New York, Inc., 1992, pp. 143–176.

14. Labrujere, Th. E.; Loeve, W.; and Sloof, J. W.: An Approximate Method for the Determination of the Pressure Distribution on Wings in the Lower Critical Speed Range. Transonic Aerodynamics. AGARD CP No. 35, Sept. 1968, pp. 17-1–17-10.

15. Allen, H. Julian; and Vincenti, Walter G.: Wall Interference in a Two-Dimensional-Flow Wind Tunnel, With Consideration of the Effect of Compressibility. NACA Rep. 782, 1944. (Supersedes NACA WR A-63.)

16. Braslow, Albert L.; and Knox, Eugene C.: Simplified Method for Determination of Critical Height of Distributed Roughness Particles for Boundary-Layer Transition at Mach Numbers From 0 to 5. NACA TN 4363, 1958.

17. Schubauer, G. B.; and Klebanoff, P. S.: Contributions on the Mechanics of Boundary-Layer Transition. NACA Rep. 1289, 1956.

TABLE I.- AIRFOIL DESIGN SPECIFICATIONS

Parameter	Objective/ Constraint	Mach Number M	Reynolds Number R	Priority
Minimum lift coefficient $c_{l,min}$	0.00^1	0.70	2.26×10^6	Low
Maximum lift coefficient $c_{l,max}$	1.25 1.20	0.30 0.40	0.97×10^6 1.29×10^6	High
Lower limit of low-drag, lift-coefficient range $c_{l,ll}$	0.10	0.70	2.26×10^6	Medium
Upper limit of low-drag, lift-coefficient range $c_{l,ul}$	0.65	0.45	1.45×10^6	Medium
Zero-lift pitching-moment coefficient $c_{m,0}$	0 ± 0.002^1 0 ± 0.005^2	0.75 0.45	2.42×10^6 1.45×10^6	High
Thickness t/c	0.14 with tab			Medium
Other requirements: Maximum lift coefficient $c_{l,max}$ independent of leading-edge roughness Docile stall characteristics 5-percent-chord tab with thickness of 0.352-percent chord				

[1]With transition fixed at 10-percent chord on upper and lower surfaces.

[2]With transition free.

TABLE II.- MODEL ORIFICE LOCATIONS

[c = 457.2 mm (18.00 in.)]

Upper Surface		Lower Surface	
x/c	y, mm (in.)	x/c	y, mm (in.)
0.0000	−129.5 (−5.10)	0.0030	−160.8 (−6.33)
.0023	−128.5 (−5.06)	.0131	−159.8 (−6.29)
.0087	−127.5 (−5.02)	.0290	−158.2 (−6.23)
.0194	−126.5 (−4.98)	.0504	−156.5 (−6.16)
.0340	−125.2 (−4.93)	.0771	−154.2 (−6.07)
.0528	−123.7 (−4.87)	.1086	−151.6 (−5.97)
.0754	−121.7 (−4.79)	.1444	−148.6 (−5.85)
.1018	−119.4 (−4.70)	.1842	−145.3 (−5.72)
.1318	−116.8 (−4.60)	.2274	−141.7 (−5.58)
.1652	−114.0 (−4.49)	.2735	−137.9 (−5.43)
.2017	−111.0 (−4.37)	.3220	−133.9 (−5.27)
.2412	−107.7 (−4.24)	.3723	−129.8 (−5.11)
.2833	−104.1 (−4.10)	.4238	−125.5 (−4.94)
.3276	−100.3 (−3.95)	.4759	−121.2 (−4.77)
.3738	−96.5 (−3.80)	.5281	−116.8 (−4.60)
.4214	−92.5 (−3.64)	.5797	−112.5 (−4.43)
.4701	−88.4 (−3.48)	.6302	−108.2 (−4.26)
.5194	−84.3 (−3.32)	.6790	−104.1 (−4.10)
.5689	−80.3 (−3.16)	.7255	−100.3 (−3.95)
.6181	−76.2 (−3.00)	.7693	−96.8 (−3.81)
.6665	−76.2 (−3.00)	.8069	−93.7 (−3.69)
.7138	−76.2 (−3.00)	.8415	−90.9 (−3.58)
.7593	−76.2 (−3.00)	.8731	−88.1 (−3.47)
.7987	−76.2 (−3.00)	.9019	−85.6 (−3.37)
.8351	−76.2 (−3.00)	.9276	−83.3 (−3.28)
.8686	−76.2 (−3.00)	.9500	−81.3 (−3.20)
.8990	−76.2 (−3.00)	.9670	−79.8 (−3.14)
.9263	−76.2 (−3.00)	.9850	−79.8 (−3.14)
.9500	−52.4 (−2.06)	.9960	−79.8 (−3.14)
.9670	−50.8 (−2.00)	1.0000	−82.8 (−3.26)
.9850	−49.2 (−1.94)		
.9960	−47.7 (−1.88)		

TABLE III.- ROUGHNESS LOCATIONS AND SIZES

R	Upper surface			Lower surface		
	x/c	Grit number	Nominal size, mm (in.)	x/c	Grit number	Nominal size, mm (in.)
0.5×10^6	0.10	30	0.711 (0.0280)	0.10	36	0.589 (0.0232)
	0.02	60	0.297 (0.0117)	0.07	30	0.711 (0.0280)
0.7×10^6	0.10	36	0.589 (0.0232)	0.10	36	0.589 (0.0232)
	0.02	80	0.211 (0.0083)	0.07	36	0.589 (0.0232)
1.0×10^6	0.10	46	0.419 (0.0165)	0.10	54	0.351 (0.0138)
	0.02	100	0.150 (0.0059)	0.07	54	0.351 (0.0138)
1.5×10^6	0.10	60	0.297 (0.0117)	0.10	70	0.249 (0.0098)
	0.02	120	0.124 (0.0049)	0.07	70	0.249 (0.0098)
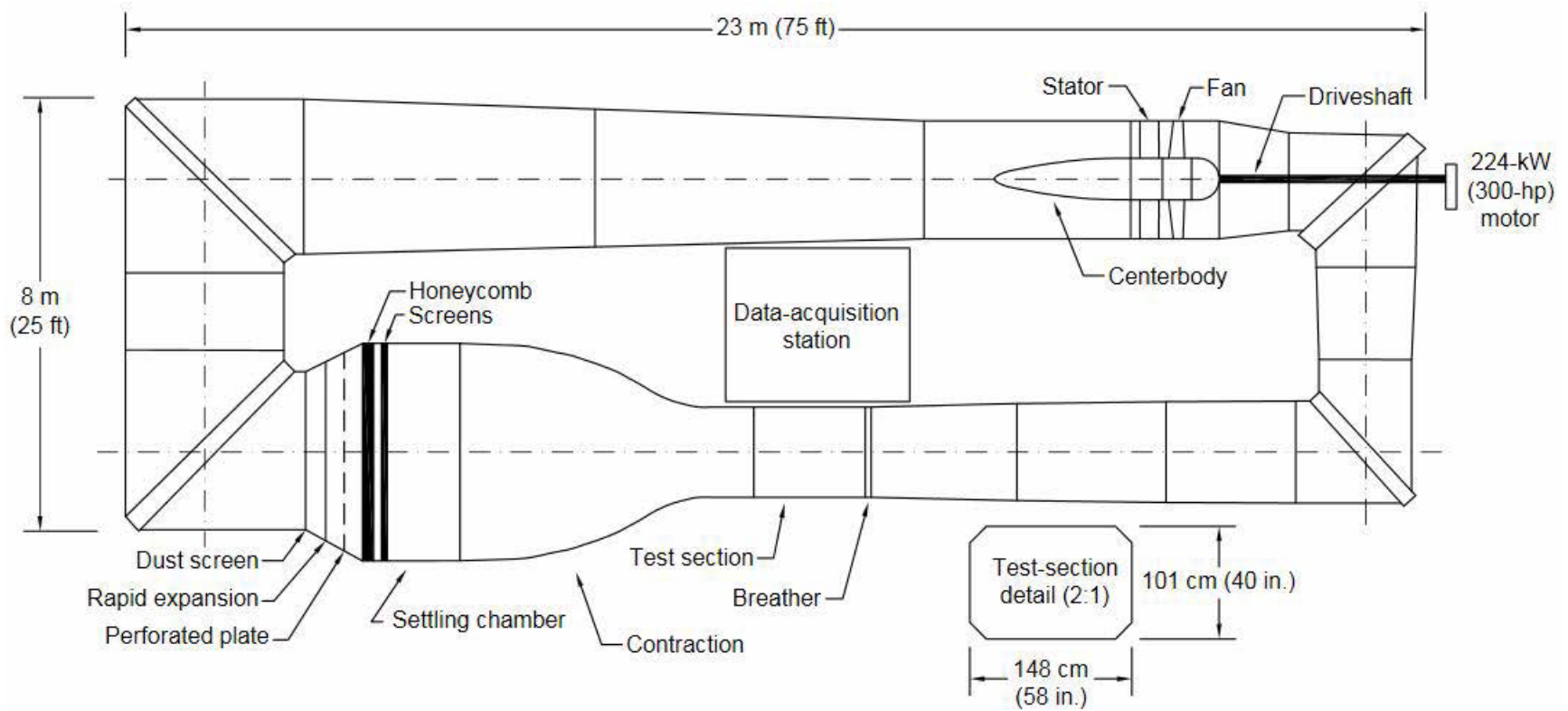
Figure 1.- The Pennsylvania State University Low-Speed, Low-Turbulence Wind Tunnel.

Figure 2.- S411 airfoil model and wake-survey probe mounted in test section.

Static-pressure connection

Total-pressure connection

6.4 mm (0.25 in.)

57.2 mm (2.25 in.)

25.4 mm (1.00 in.)

1.60 mm (0.063 in.)

5 equally spaced orifices,
0.64-mm (0.025-in.) diameter
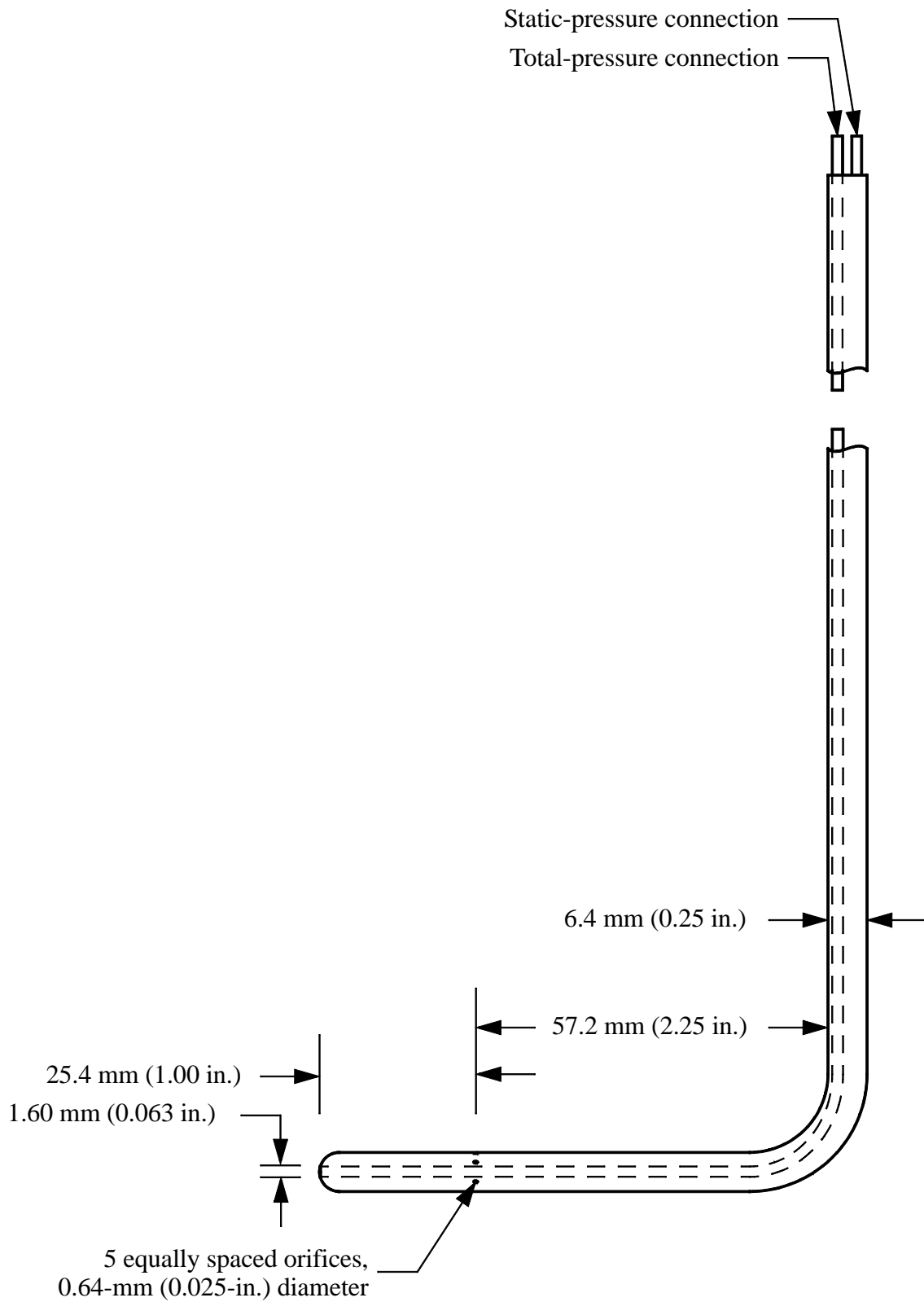
Figure 3.- Wake-survey probe.
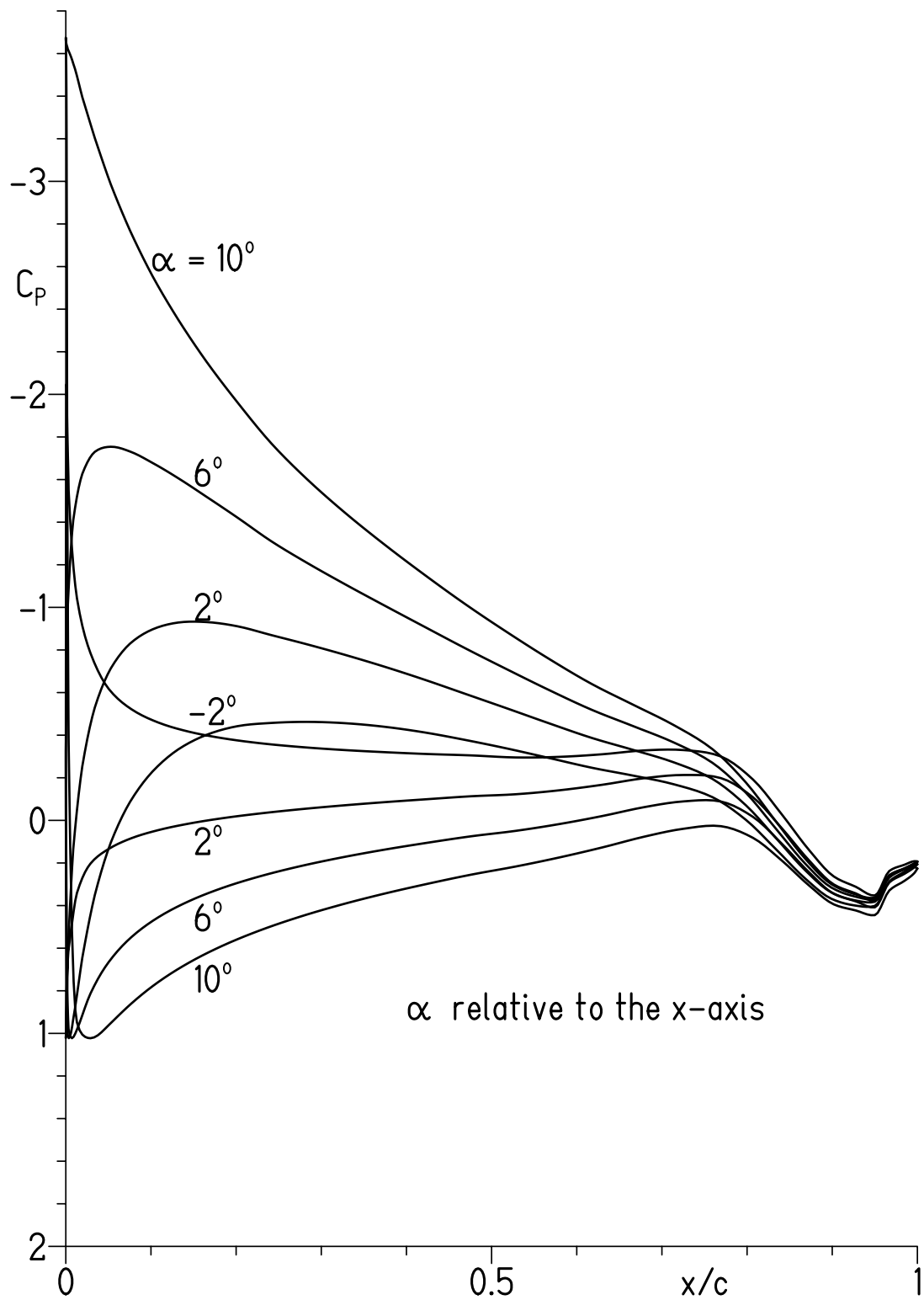
(a) M = 0.30.

Figure 4.- Theoretical (inviscid) pressure distributions.
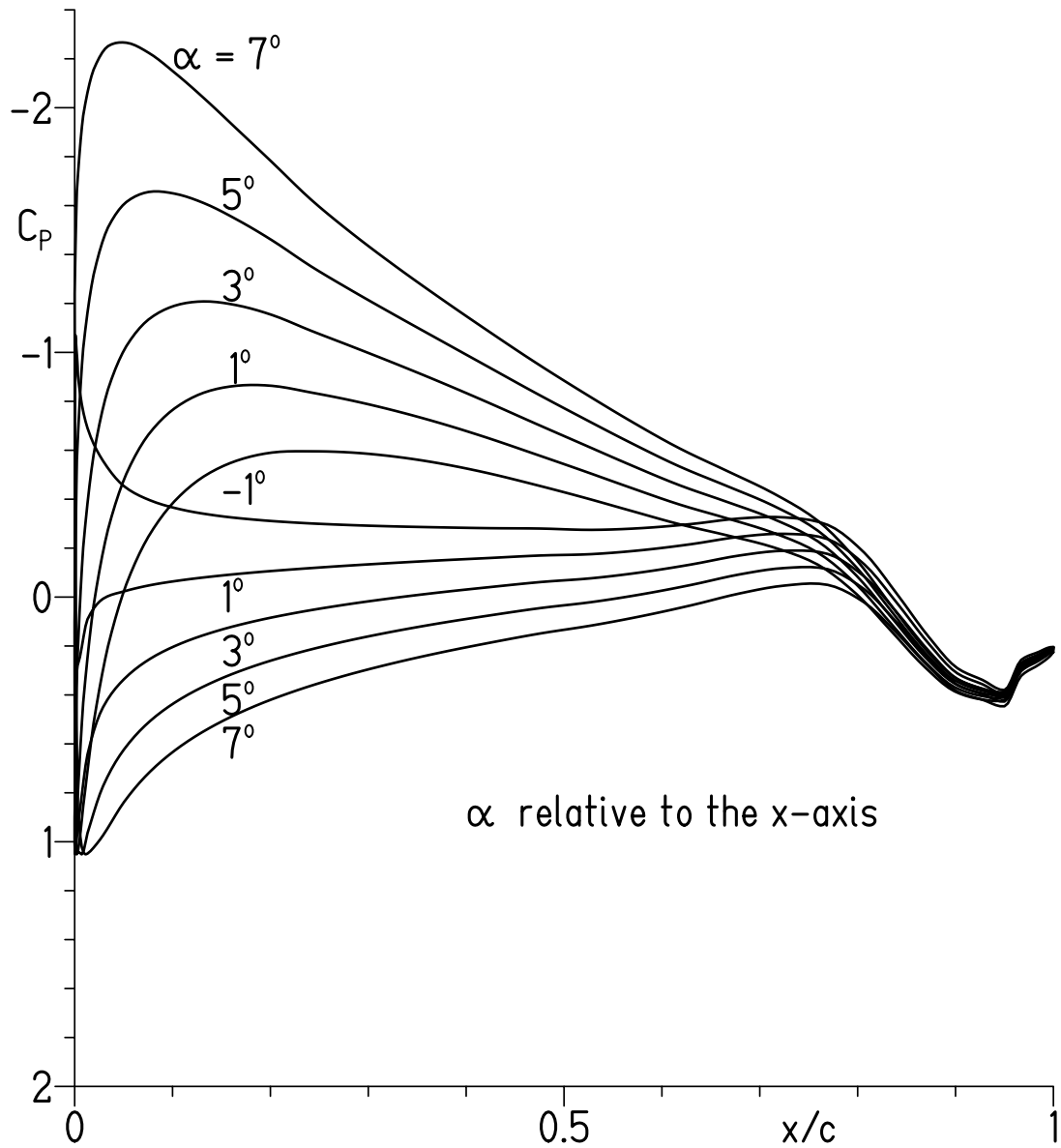
(b) M = 0.45.

Figure 4.- Concluded.
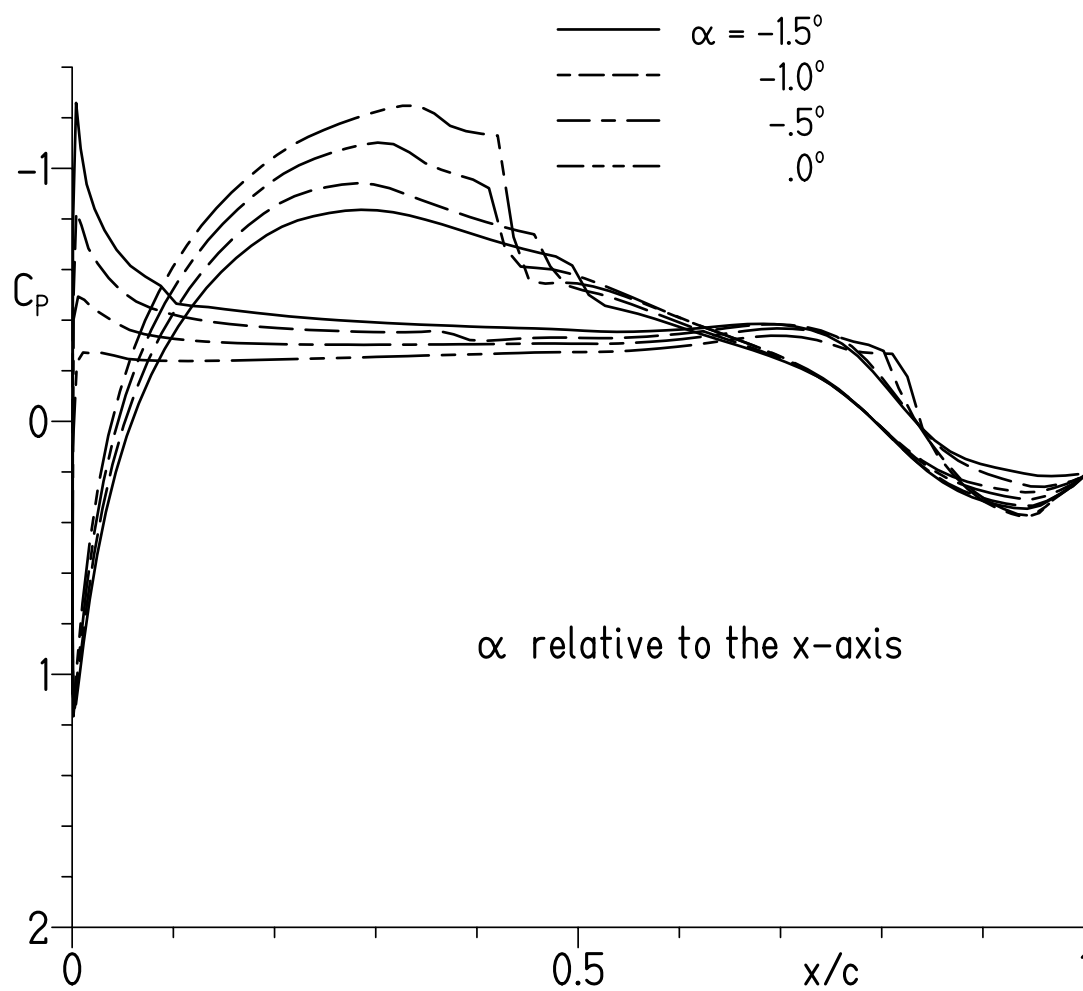
Figure 5.- Theoretical pressure distributions at $M = 0.70$ and $R = 2.26 \times 10^6$ with transition free.

PROFIL07

MSES 3.0
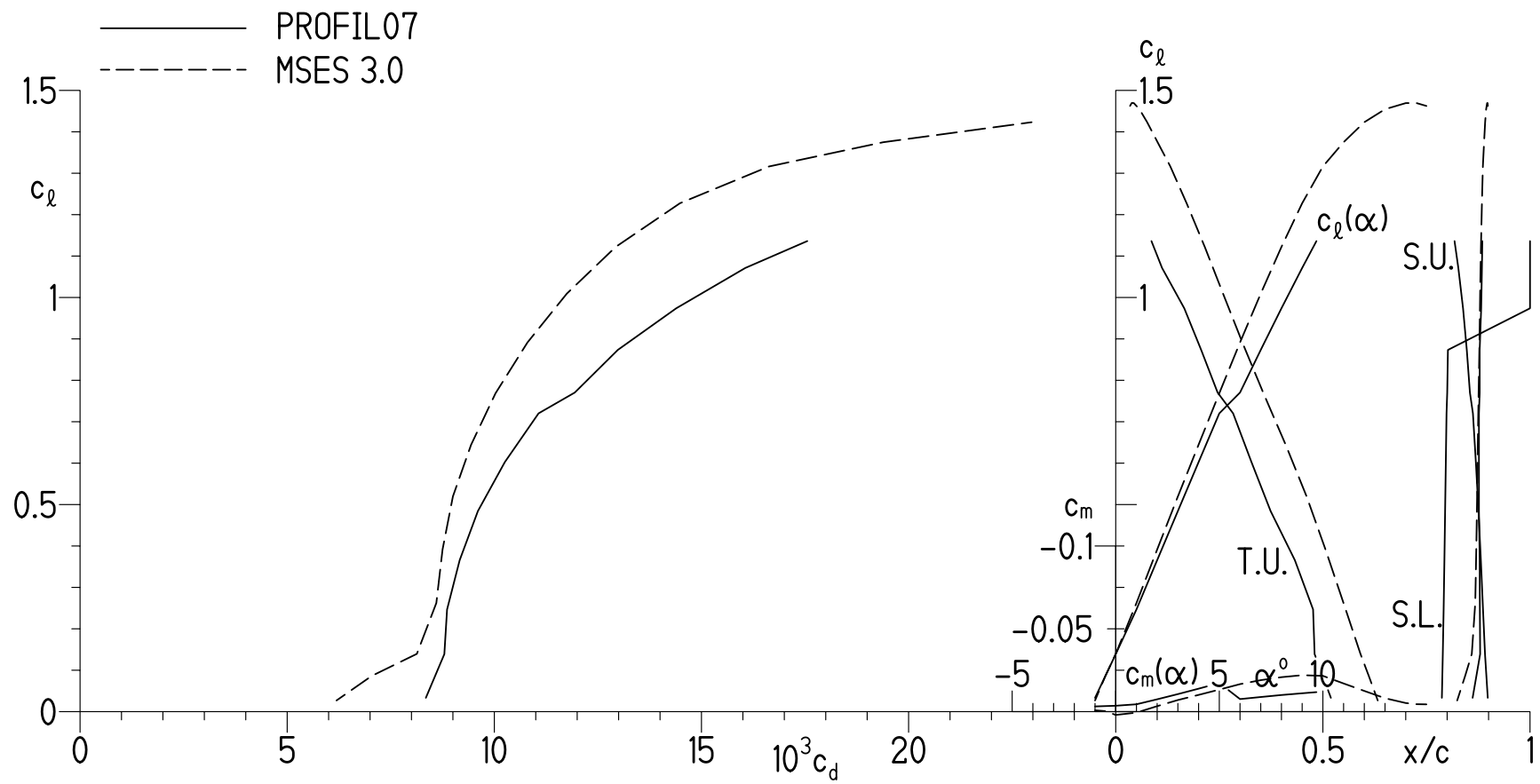
(a) Transition free.

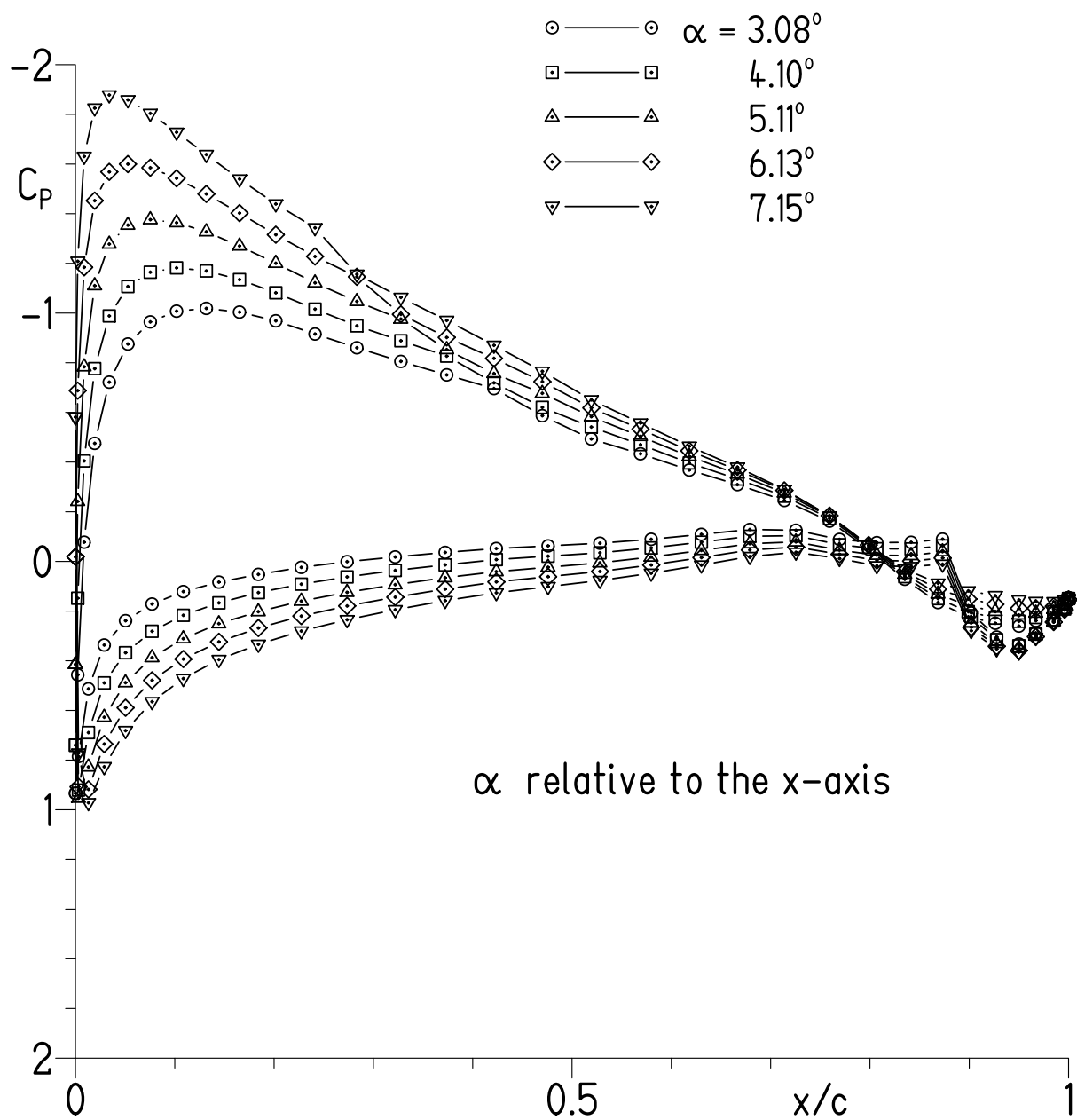Figure 6.- Theoretical section characteristics at $M = 0.30$ and $R = 0.97 \times 10^6$.
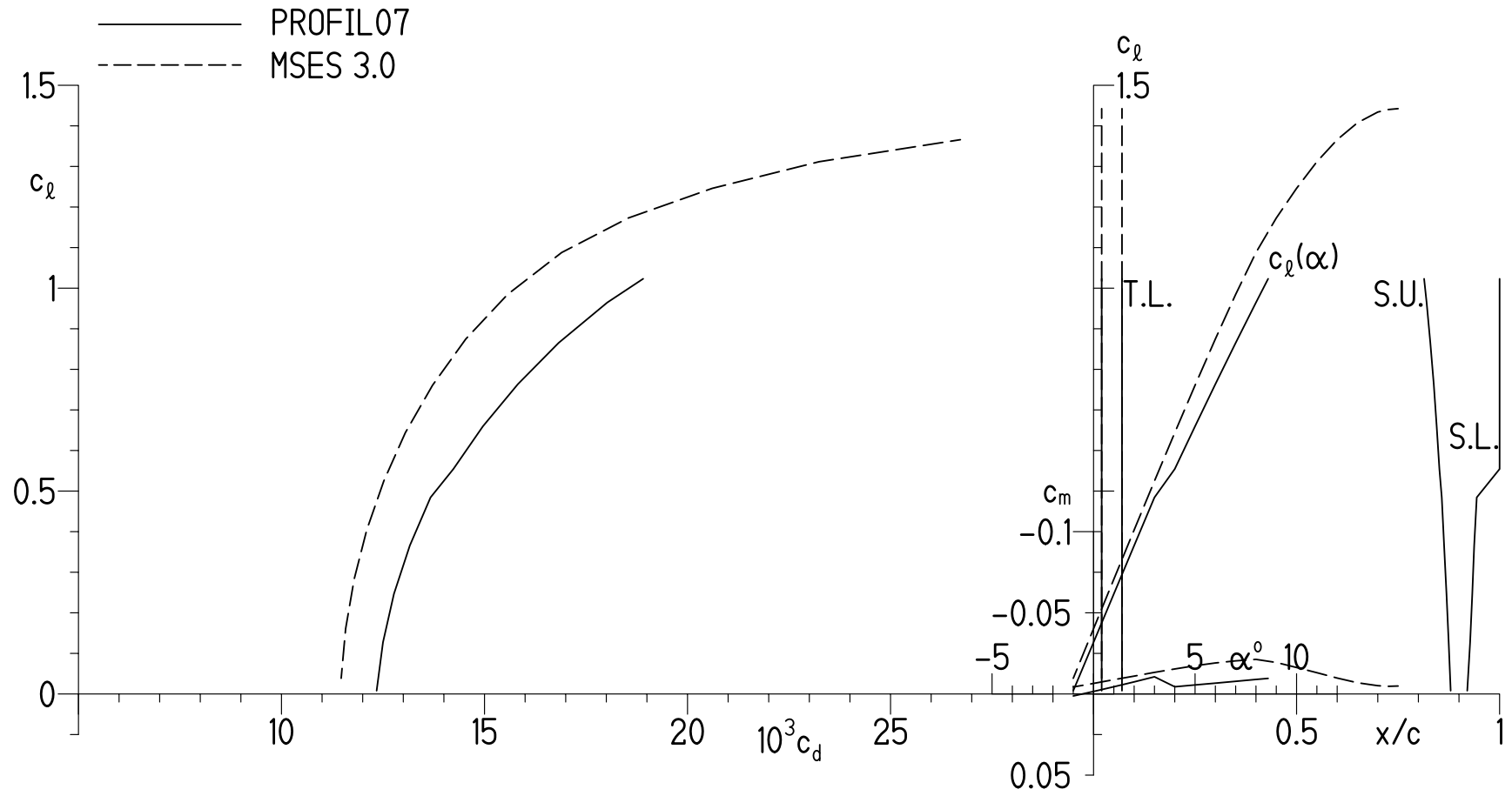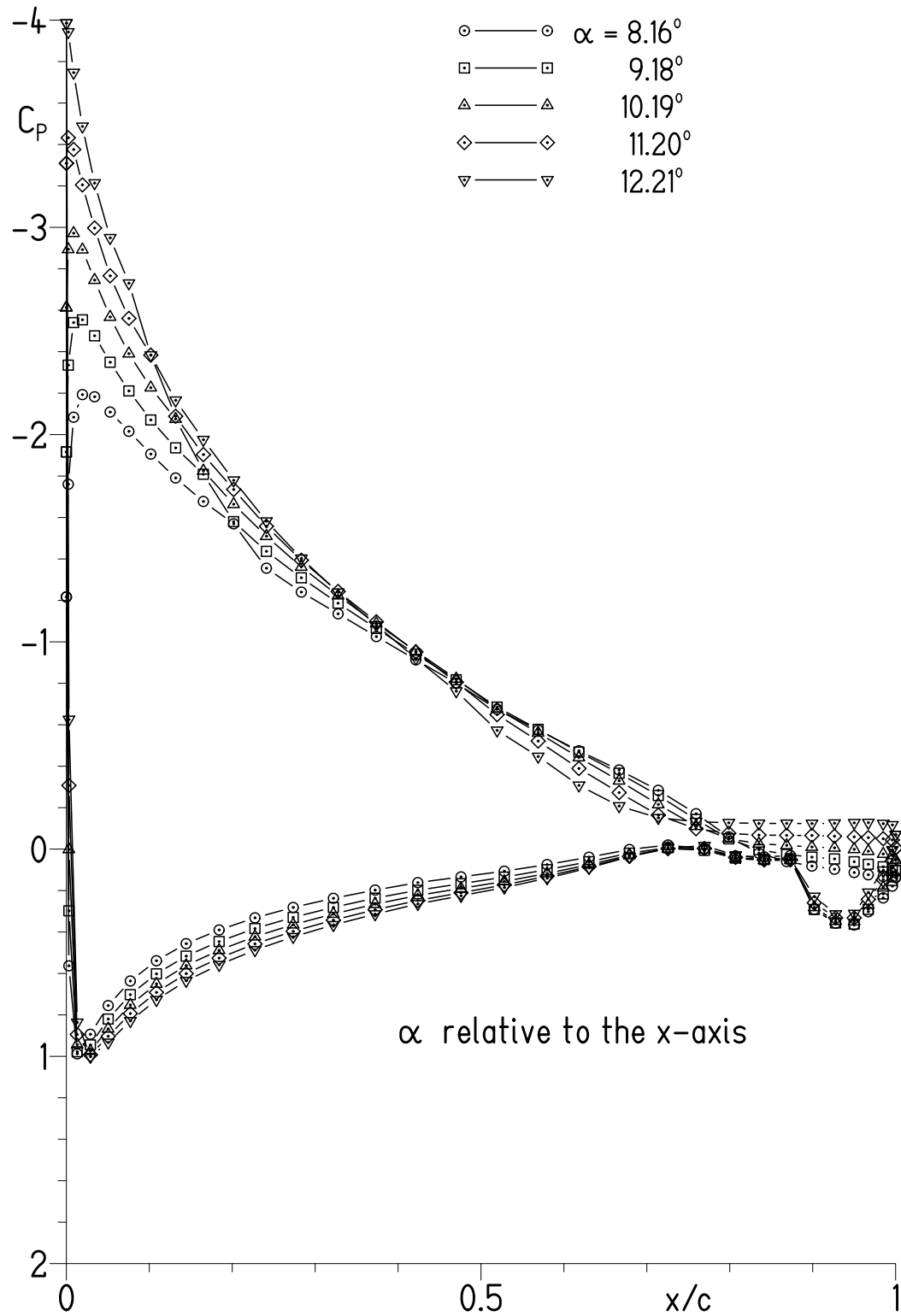
(b) Transition fixed.

Figure 6.- Concluded.
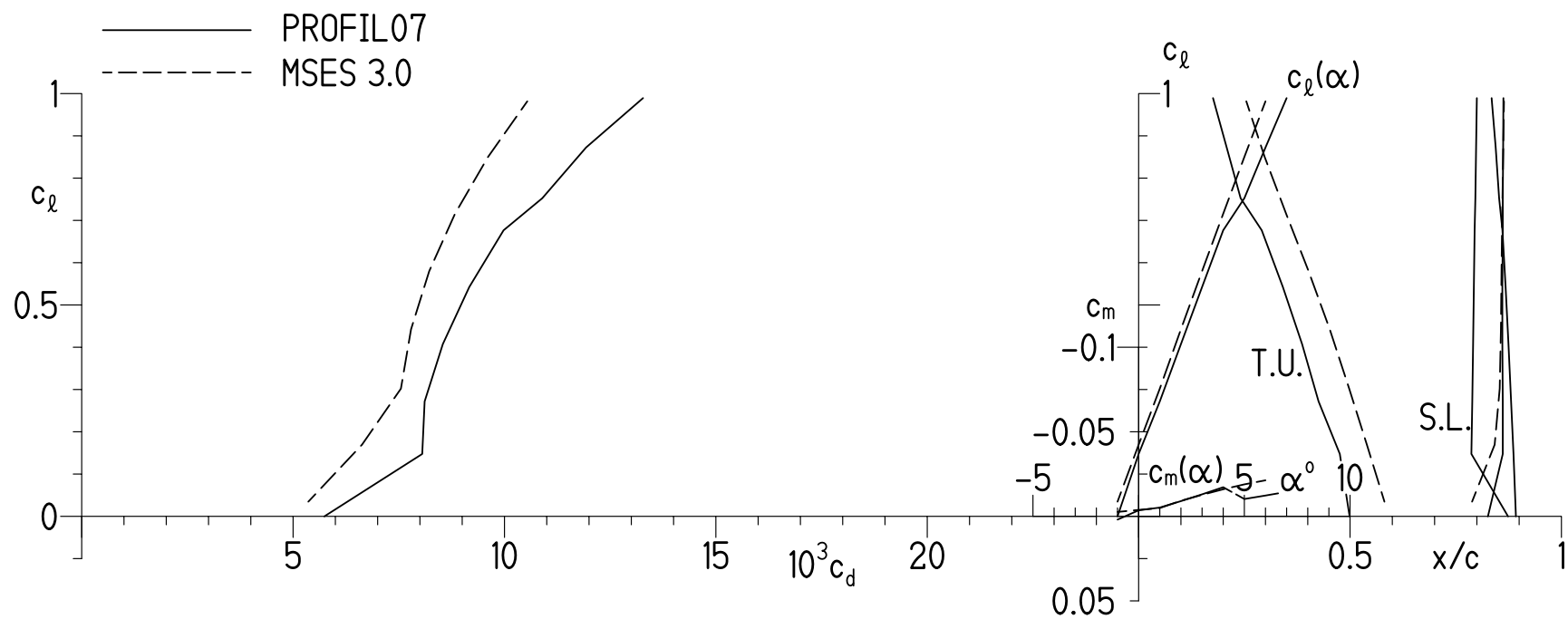
(a) Transition free.

Figure 7.- Theoretical section characteristics at $M = 0.45$ and $R = 1.45 \times 10^6$.
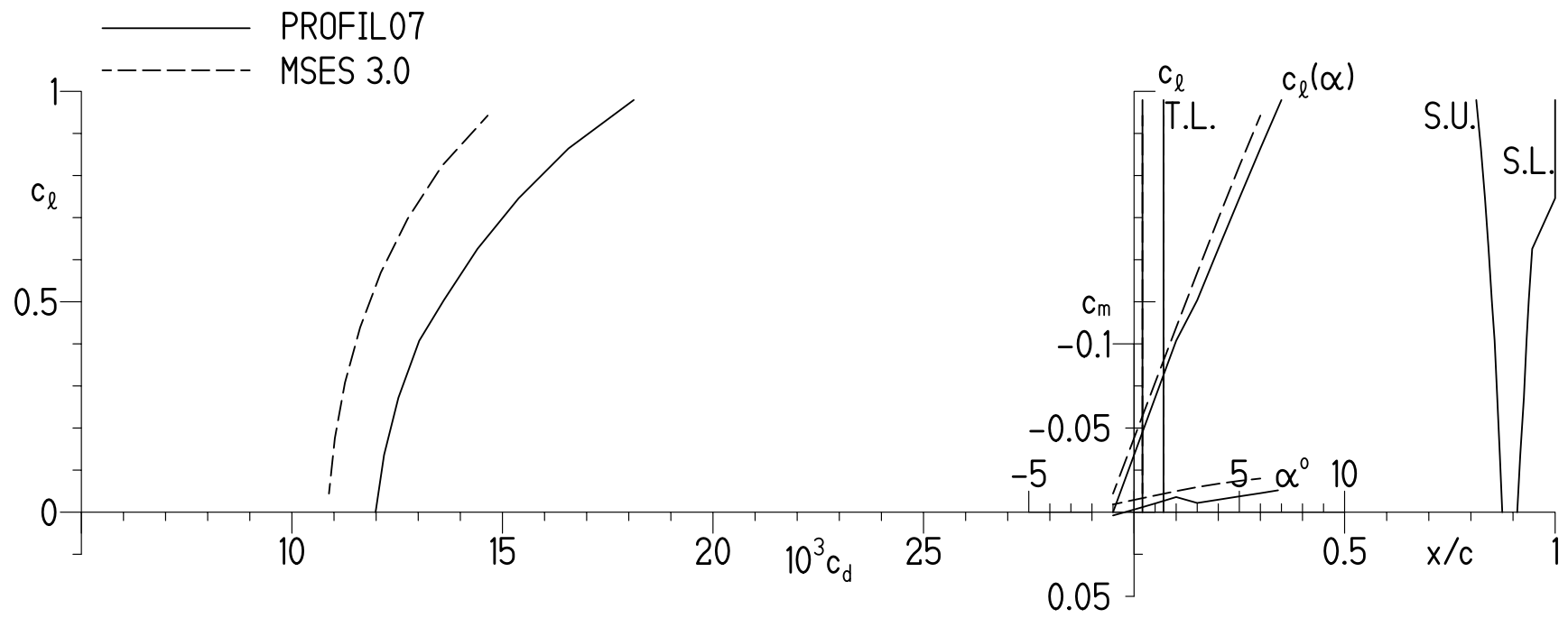
(b) Transition fixed.

Figure 7.- Concluded.

MSES 3.0

c_ℓ

c_ℓ

$10^3 c_d$

c_m

c_ℓ

α^o

x/c
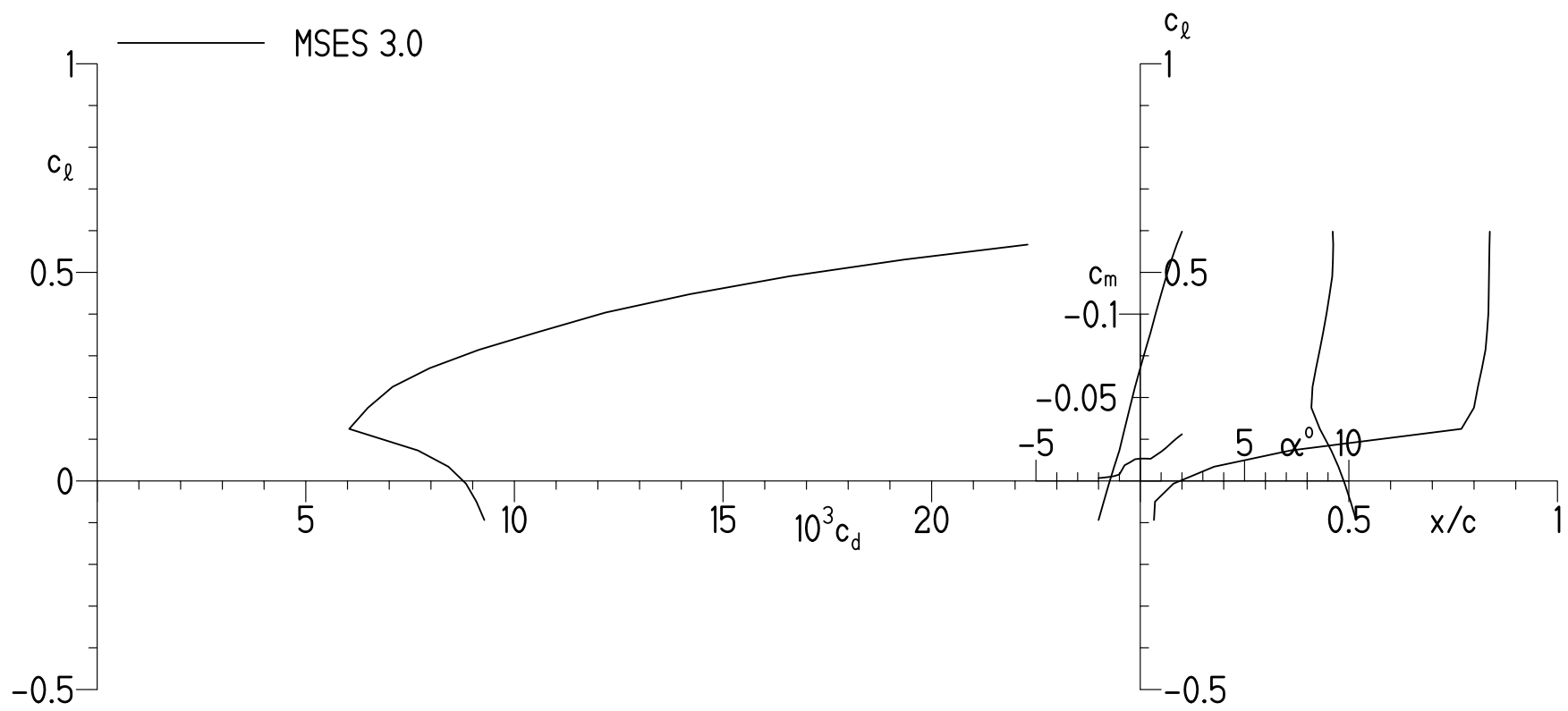
(a) Transition free.

Figure 8.- Theoretical section characteristics at $M = 0.70$ and $R = 2.26 \times 10^6$.
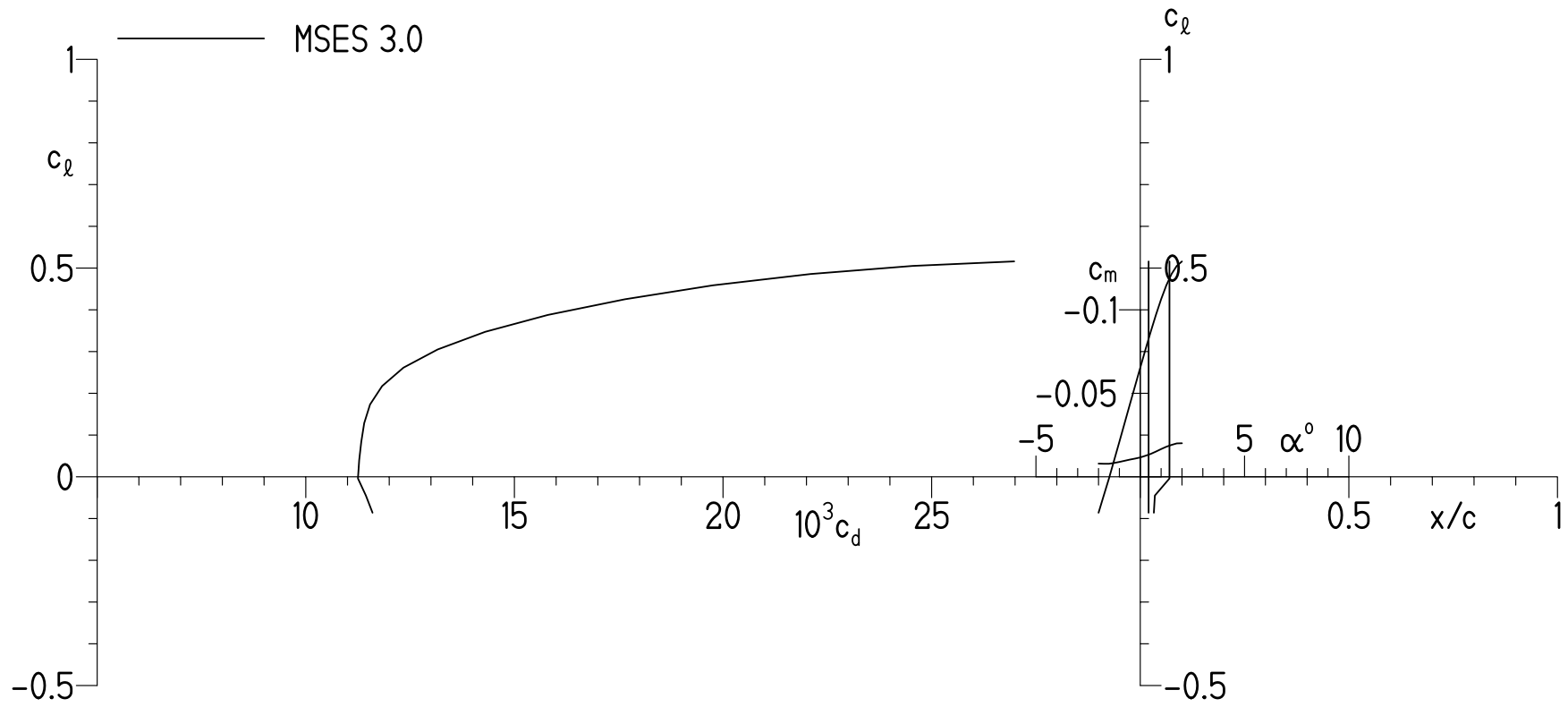
(b) Transition fixed.

Figure 8.- Concluded.
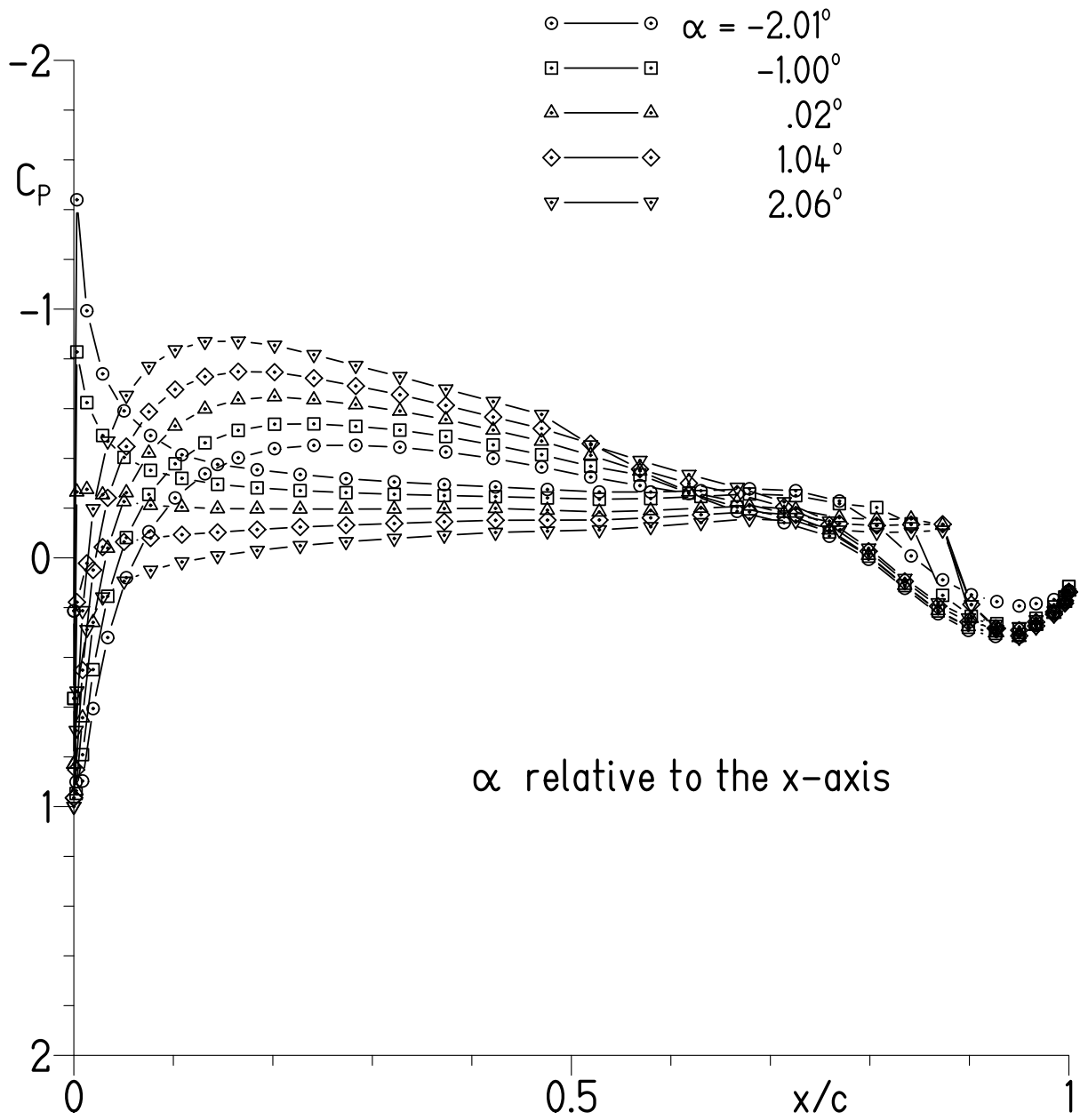
(a) α = −2.01°, −1.00°, 0.02°, 1.04°, and 2.06°.

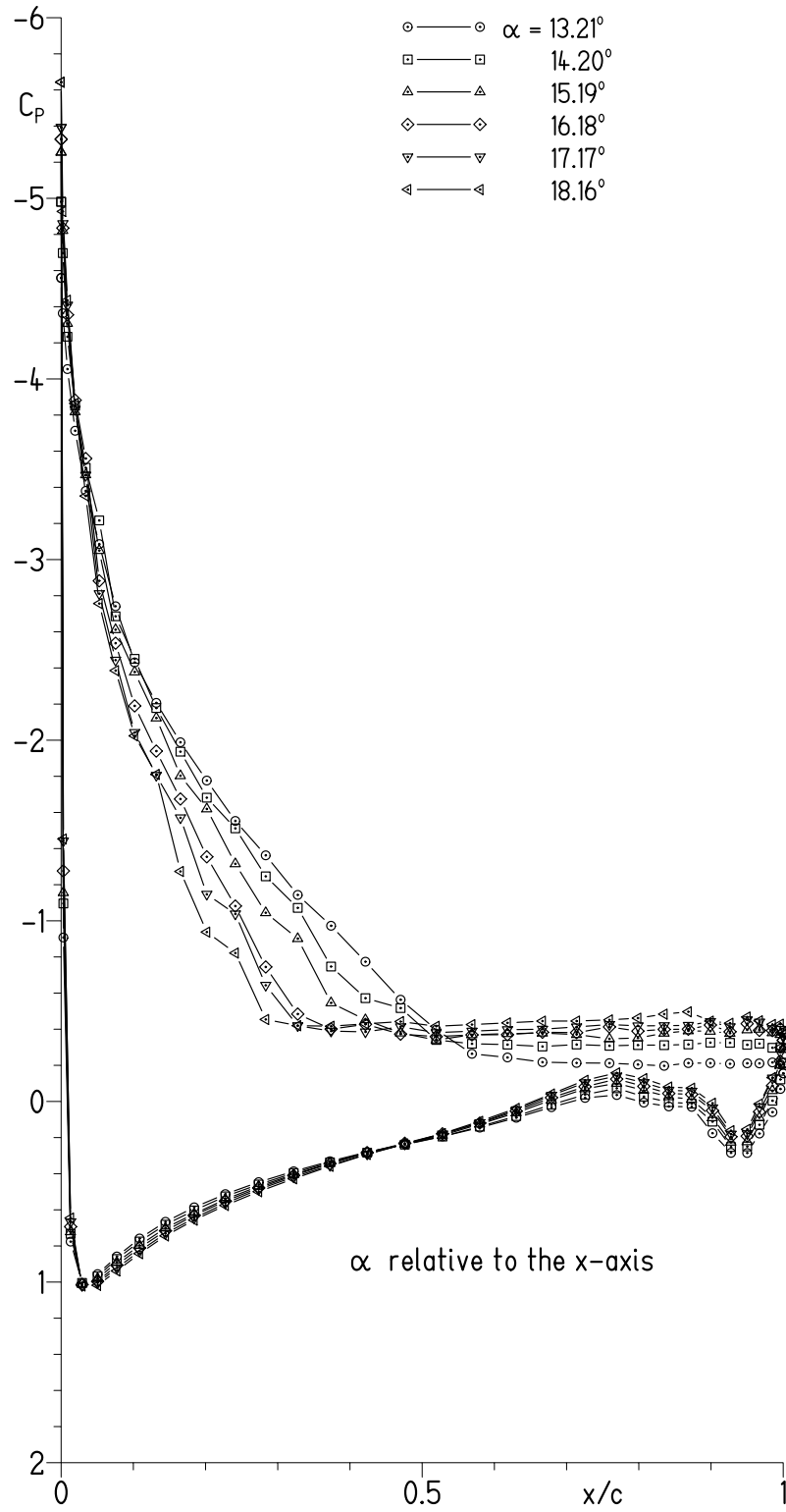Figure 9.- Experimental pressure distributions for $R = 1.00 \times 10^6$ and $M = 0.10$ with transition free.

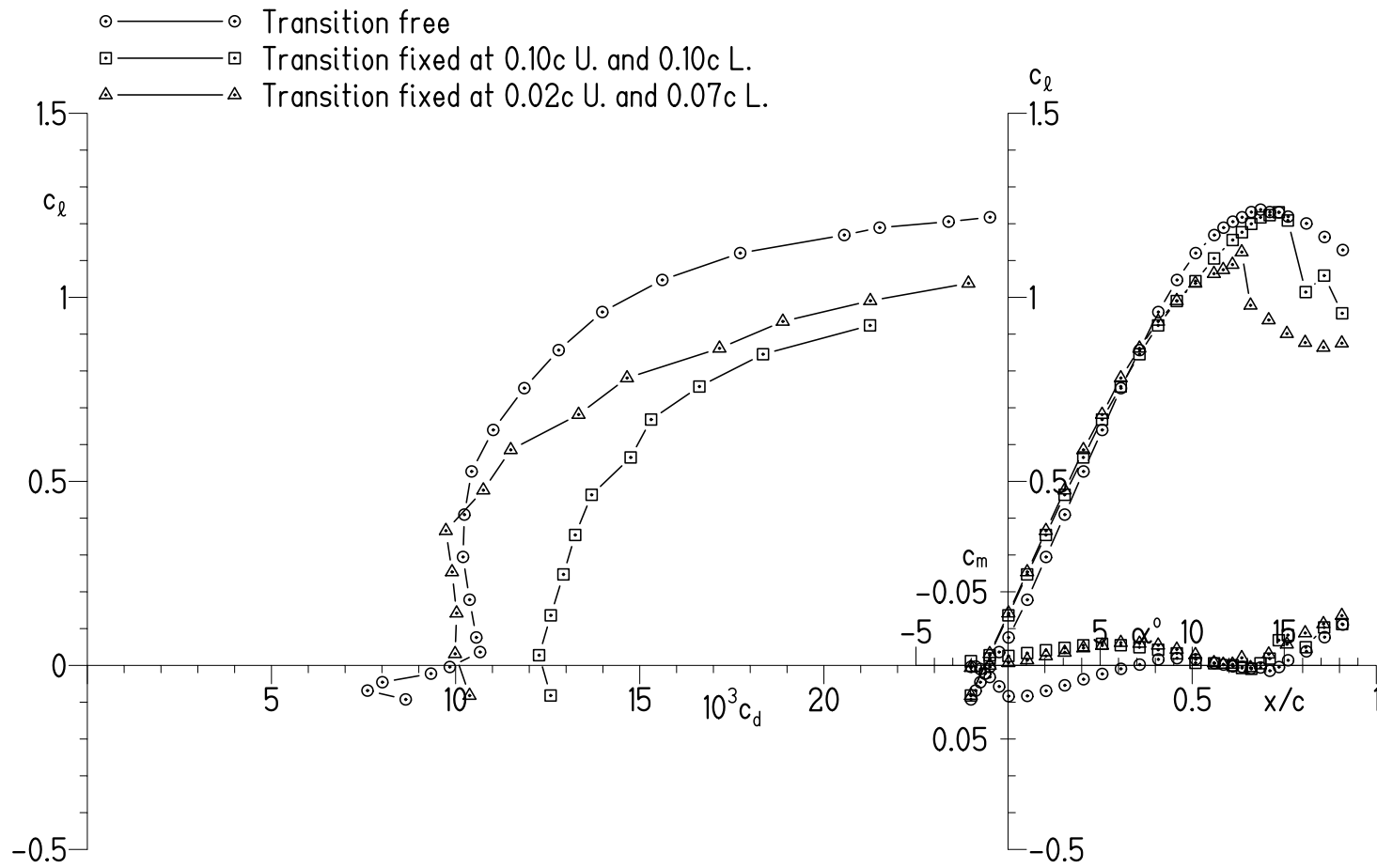(b) α = 3.08°, 4.10°, 5.11°, 6.13°, and 7.15°.

Figure 9.- Continued.

(c) $\alpha = 8.16°$, $9.18°$, $10.19°$, $11.20°$, and $12.21°$.

Figure 9.- Continued.

(d) $\alpha = 13.21°$, $14.20°$, $15.19°$, $16.18°$, $17.17°$, and $18.16°$.
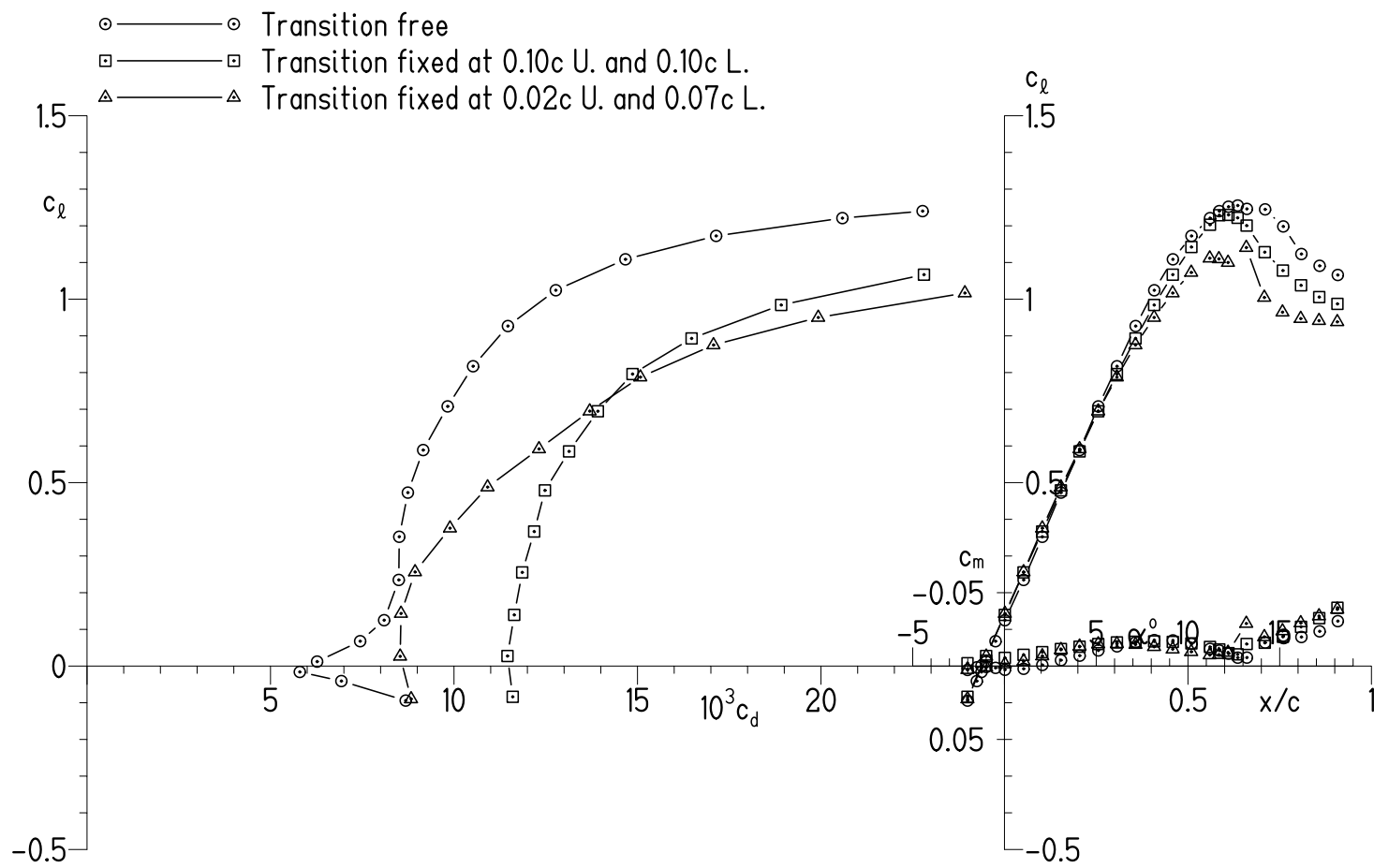
Figure 9.- Concluded.

(a) $R = 0.50 \times 10^6$ and $M = 0.05$.

Figure 10.- Experimental section characteristics with transition free and transition fixed.
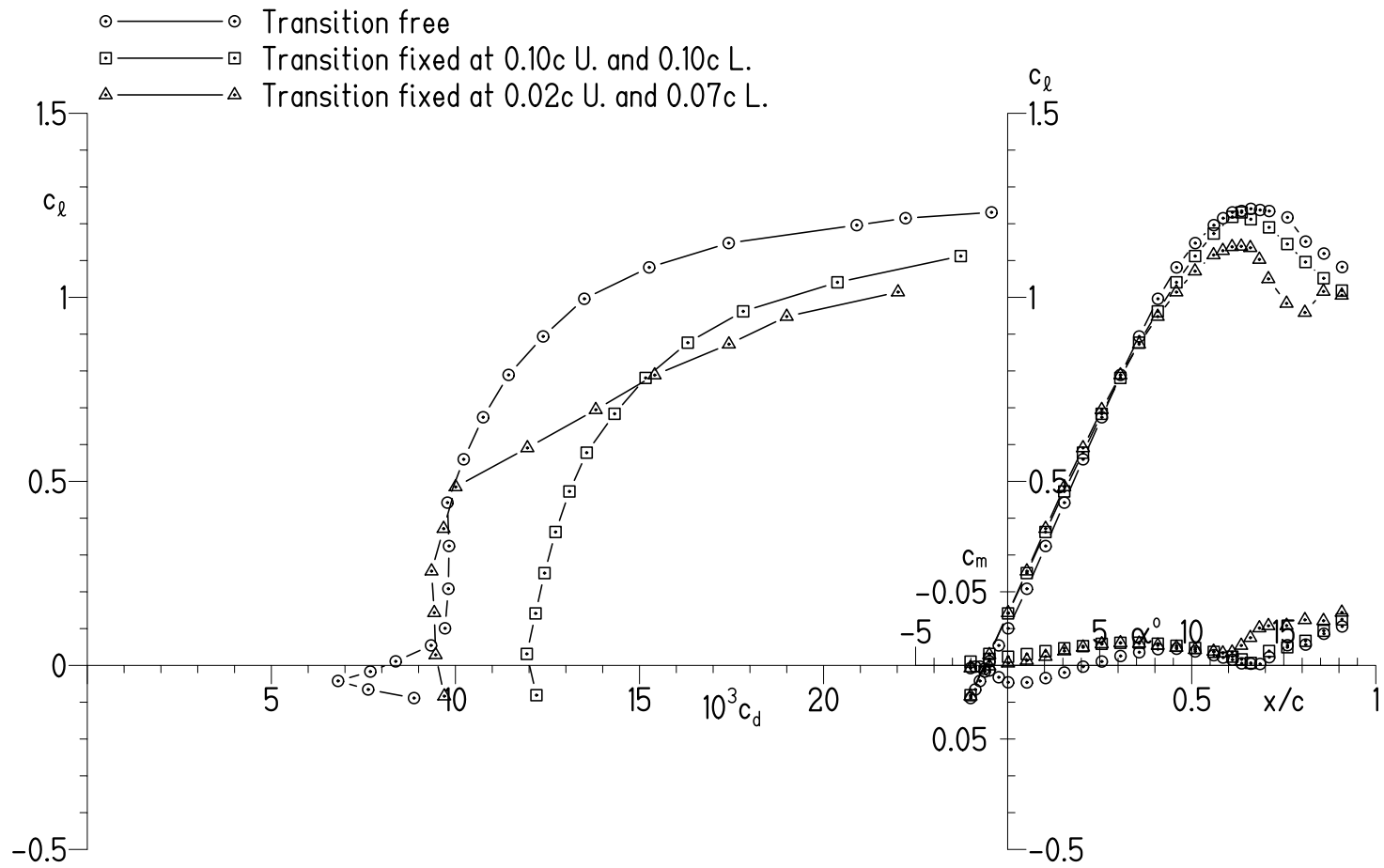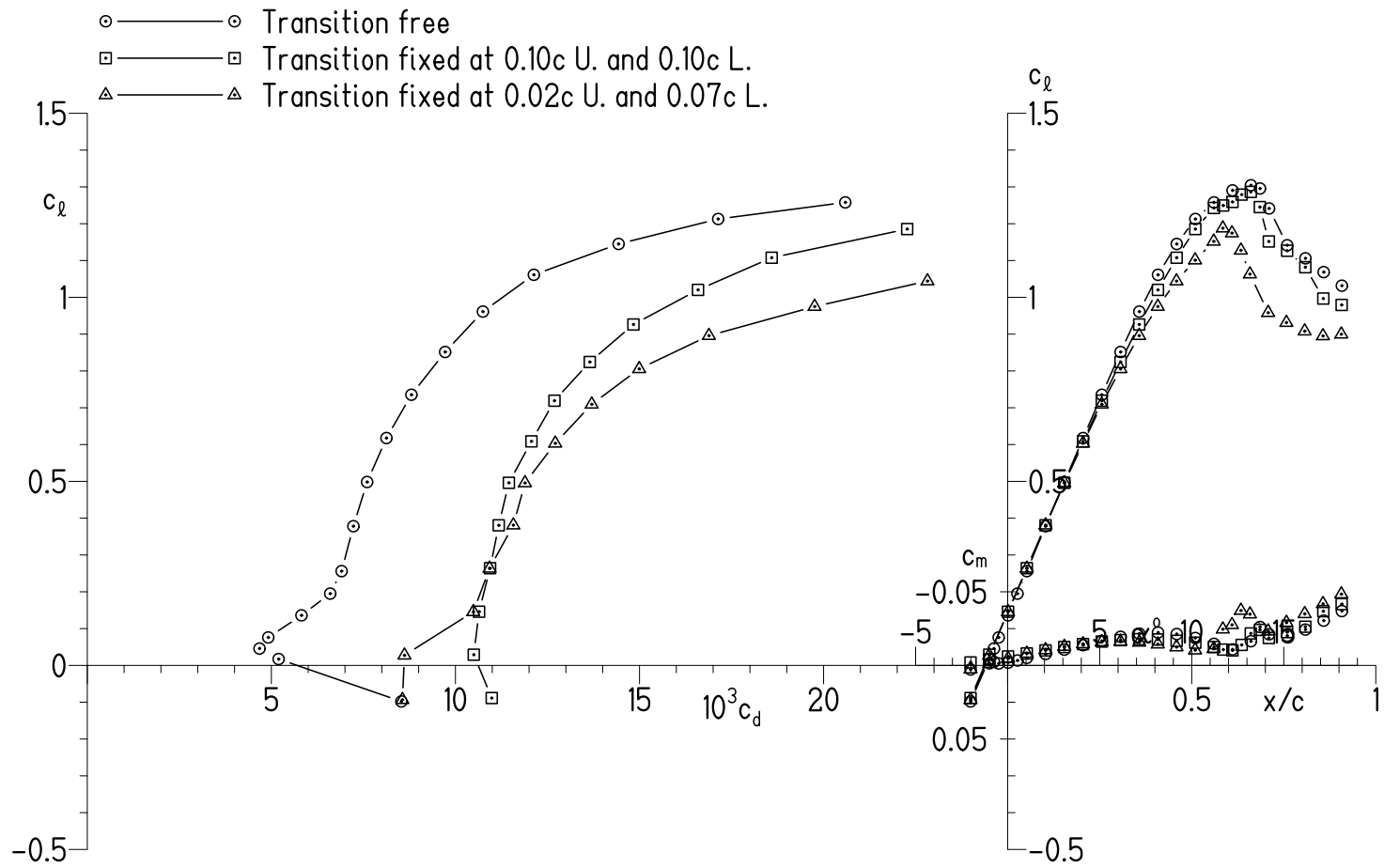
(b) $R = 0.70 \times 10^6$ and $M = 0.07$.

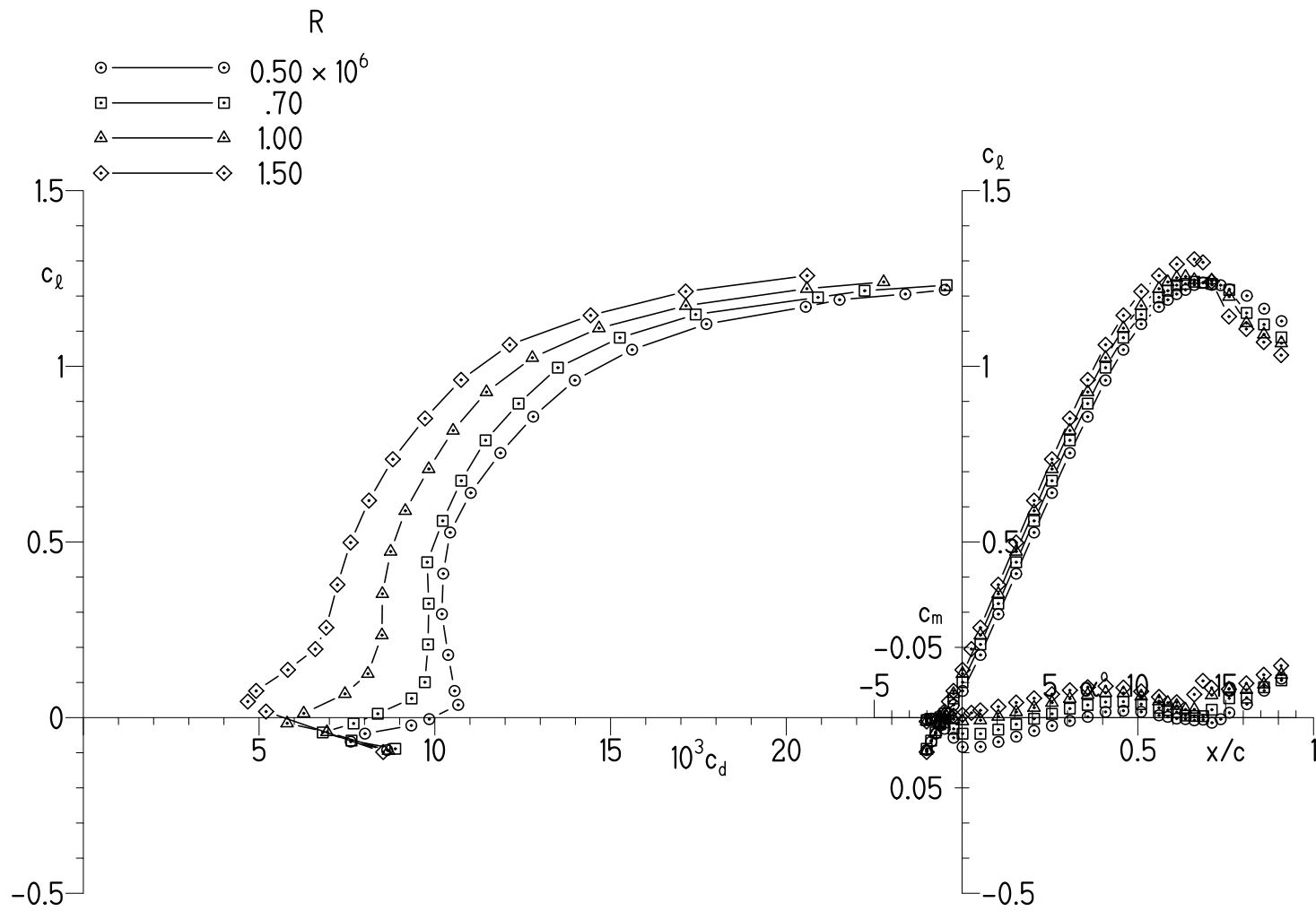Figure 10.- Continued.

Transition free
Transition fixed at 0.10c U. and 0.10c L.
Transition fixed at 0.02c U. and 0.07c L.

(c) $R = 1.00 \times 10^6$ and $M = 0.10$.

Figure 10.- Continued.

(d) R = 1.5 × 10^6 and M = 0.16.

Figure 10.- Concluded.

R

⊙———⊙ 0.50×10^6
⊡———⊡ .70
△———△ 1.00
◇———◇ 1.50

c_ℓ

1.5

c_ℓ

1

0.5

0

$10^3 c_d$

c_ℓ

1.5

1

0.5

c_m
−0.05

−0.5

0.05

−0.5

0.5   x/c   1

(a) Transition free.

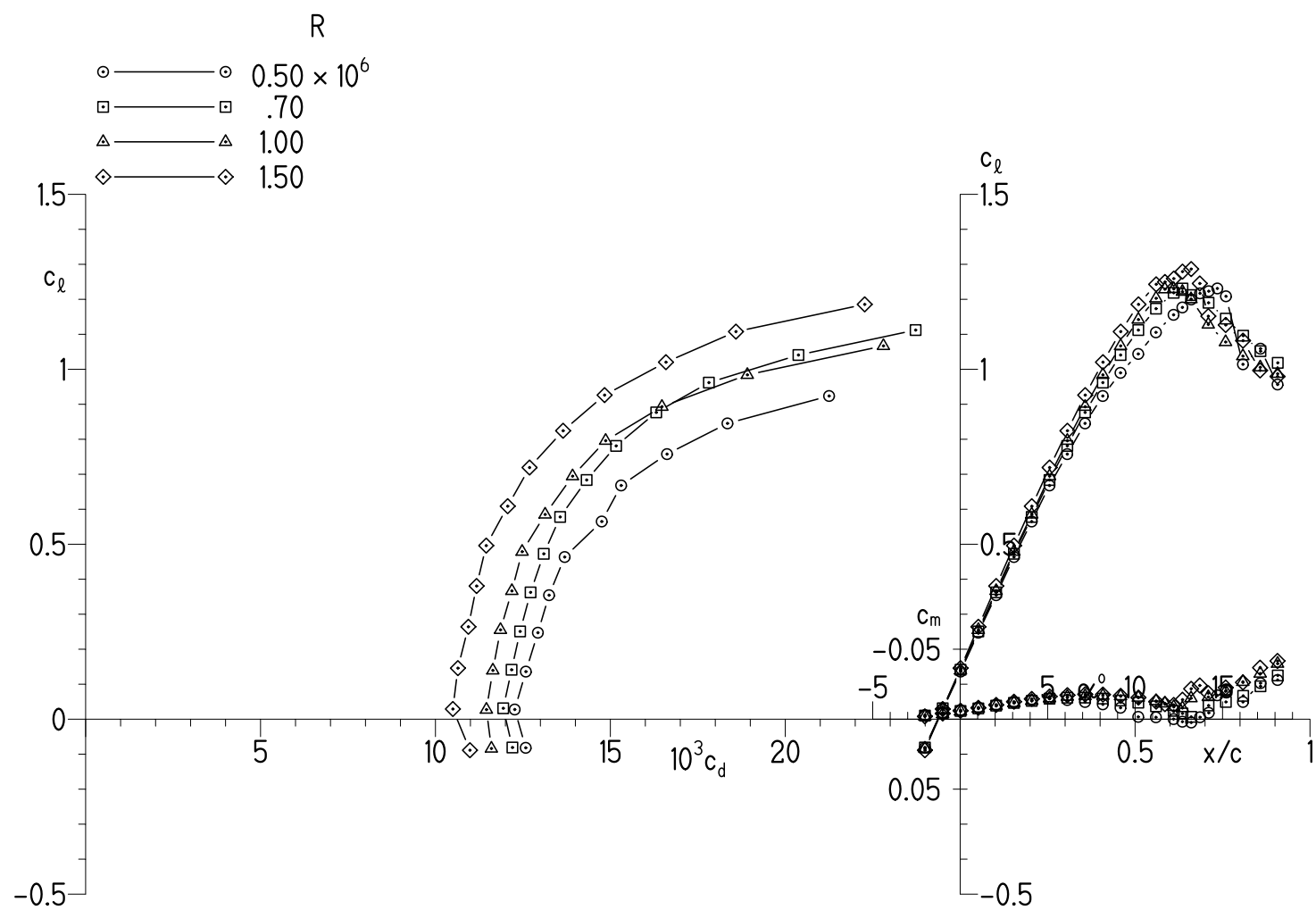Figure 11.- Effects of Reynolds number on experimental section characteristics.

(b) Transition fixed at 0.10c U. and 0.10c L.
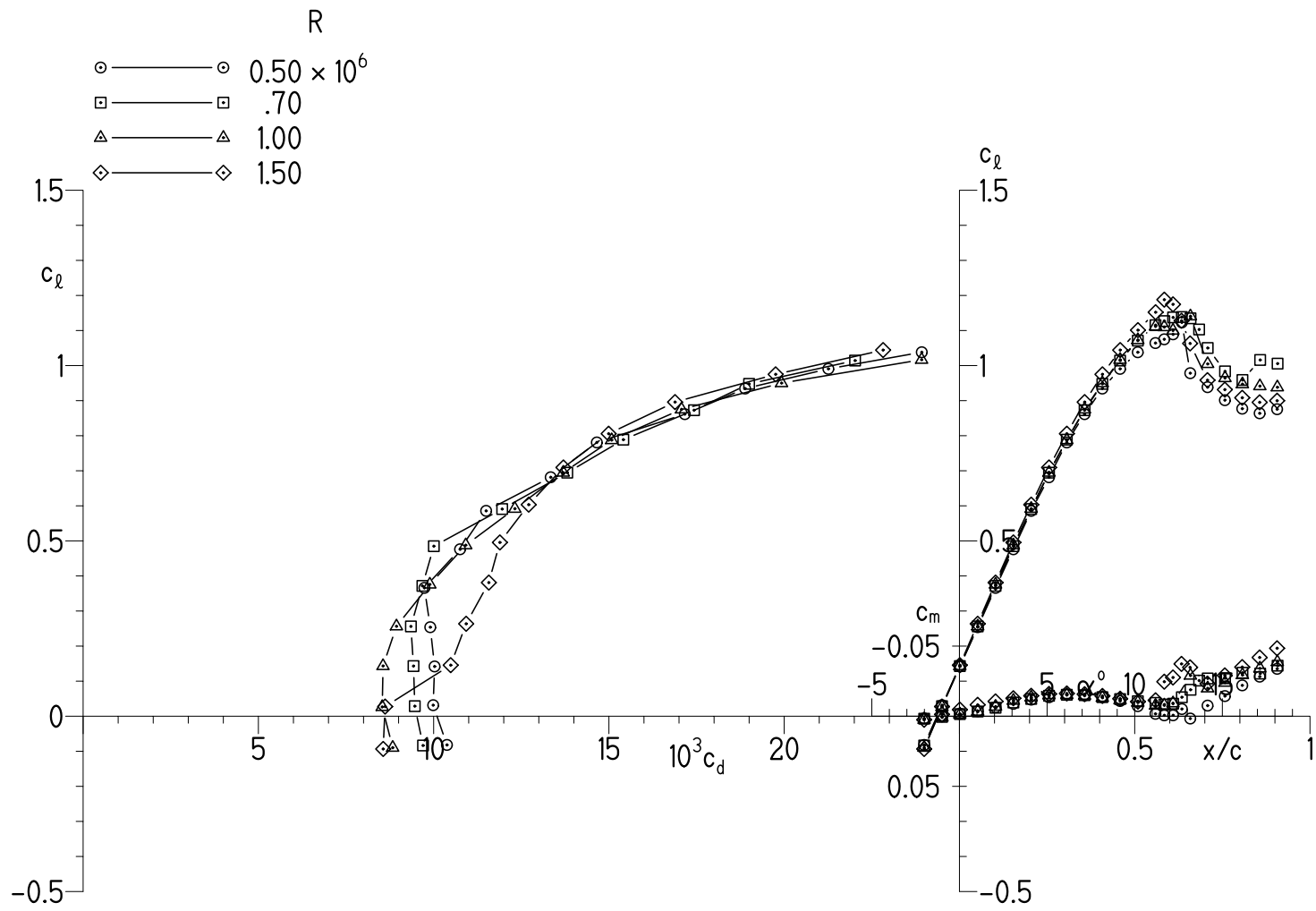
Figure 11.- Continued.

(c) Transition fixed at 0.02c U. and 0.07c L.

Figure 11.- Concluded.
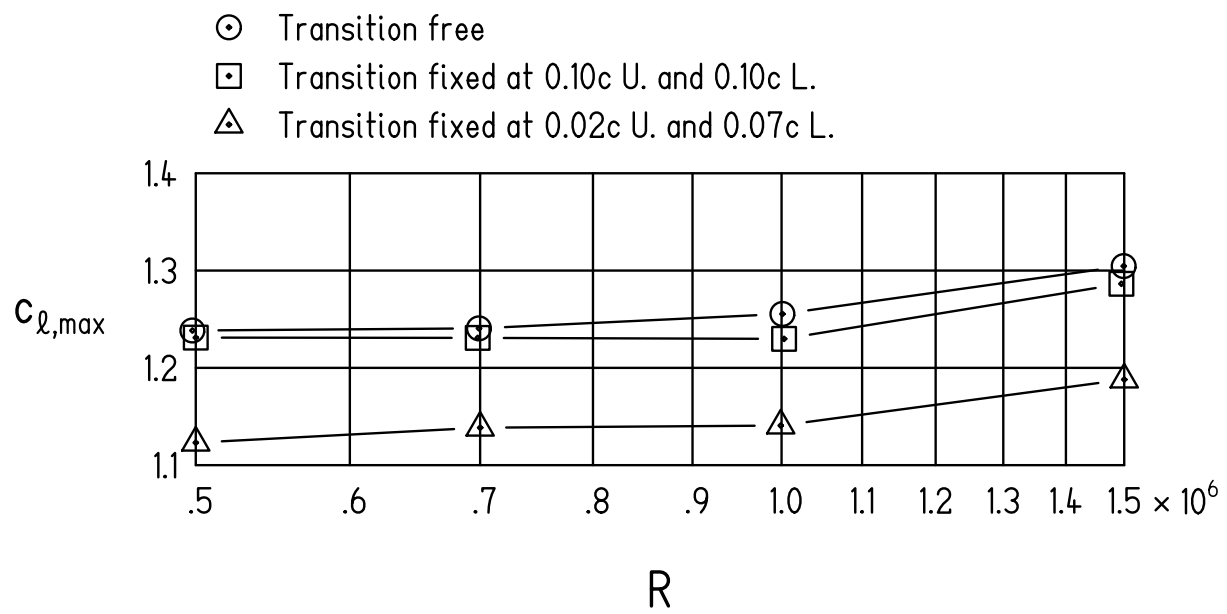
Figure 12.- Variation of experimental maximum lift coefficient with Reynolds number.
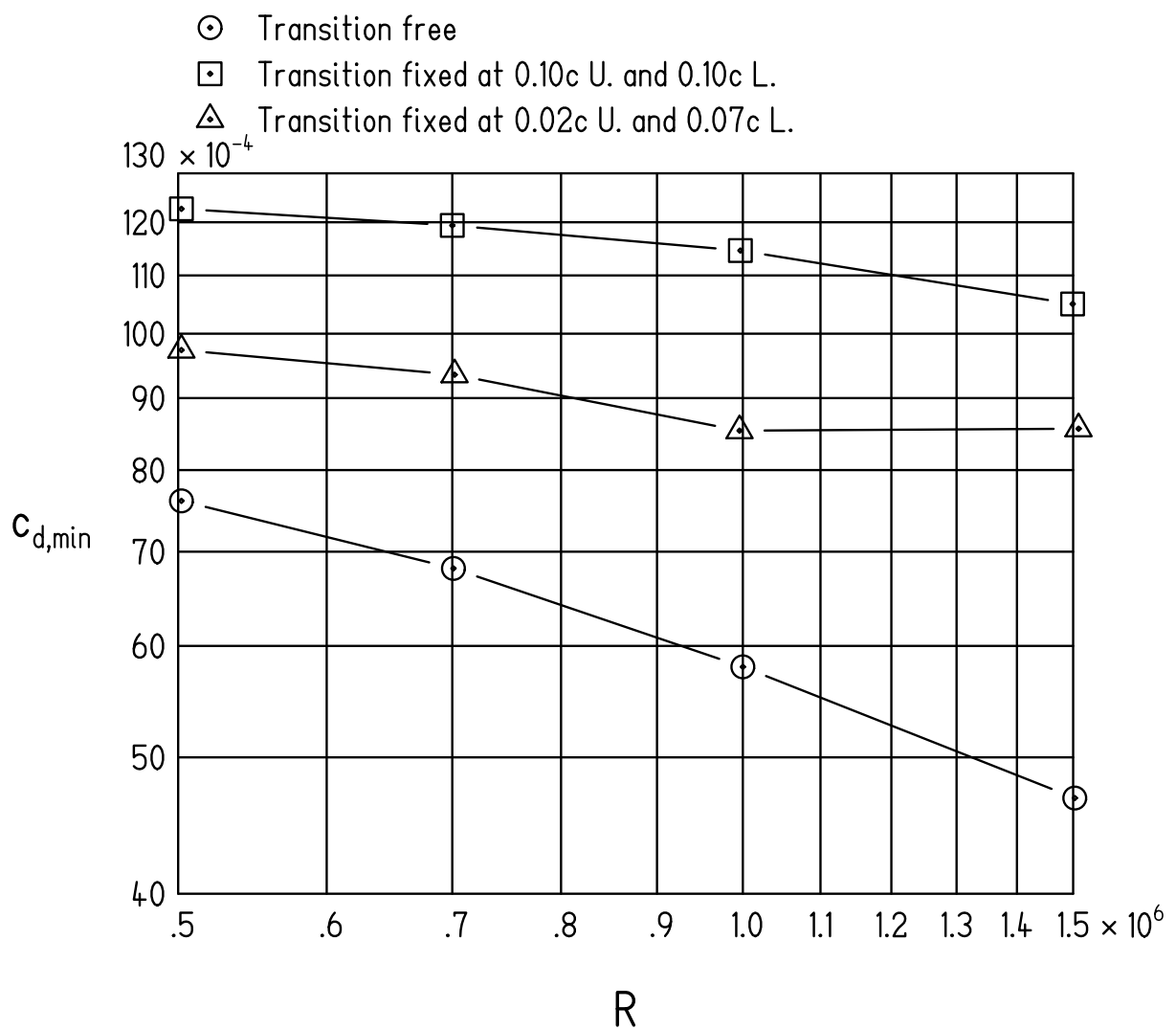
Figure 13.- Variation of experimental minimum profile-drag coefficient with Reynolds number.
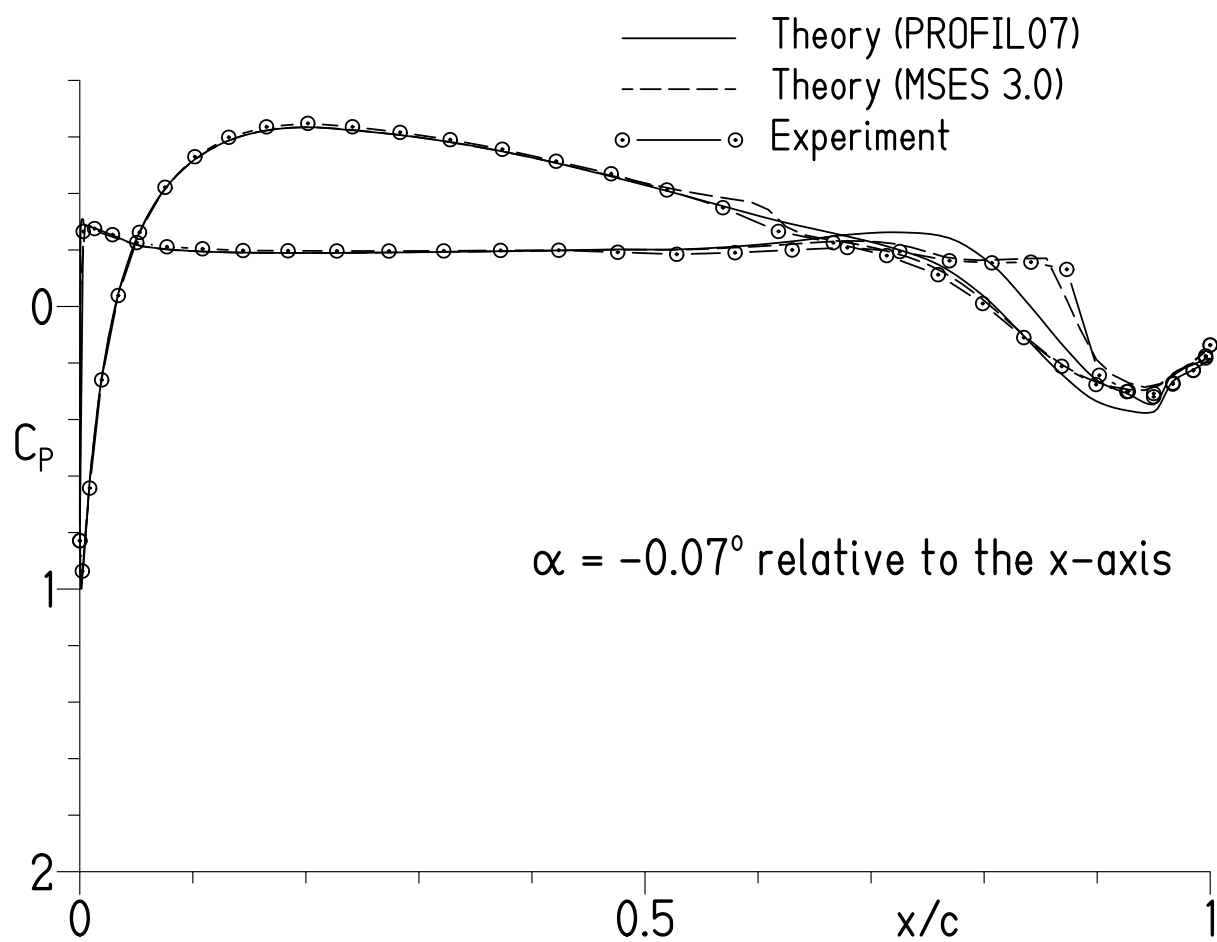
(a) $c_l = 0.13$.

Figure 14.- Comparison of theoretical and experimental pressure distributions.

Theory (PROFIL07)
Theory (MSES 3.0)
Experiment

$\alpha = 4.39°$ relative to the x-axis

C_P
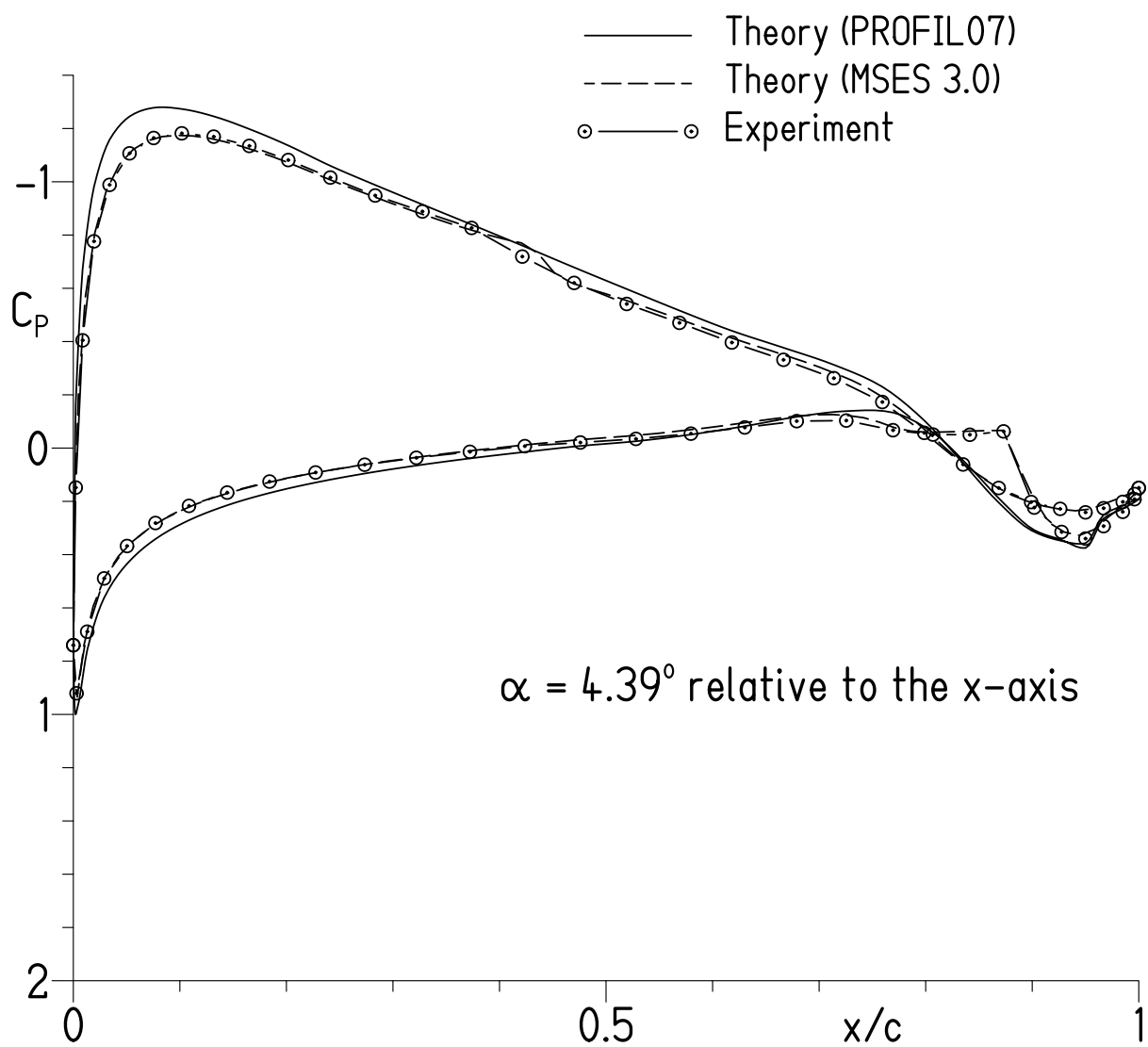
(b) $c_l = 0.61$.

Figure 14.- Continued.
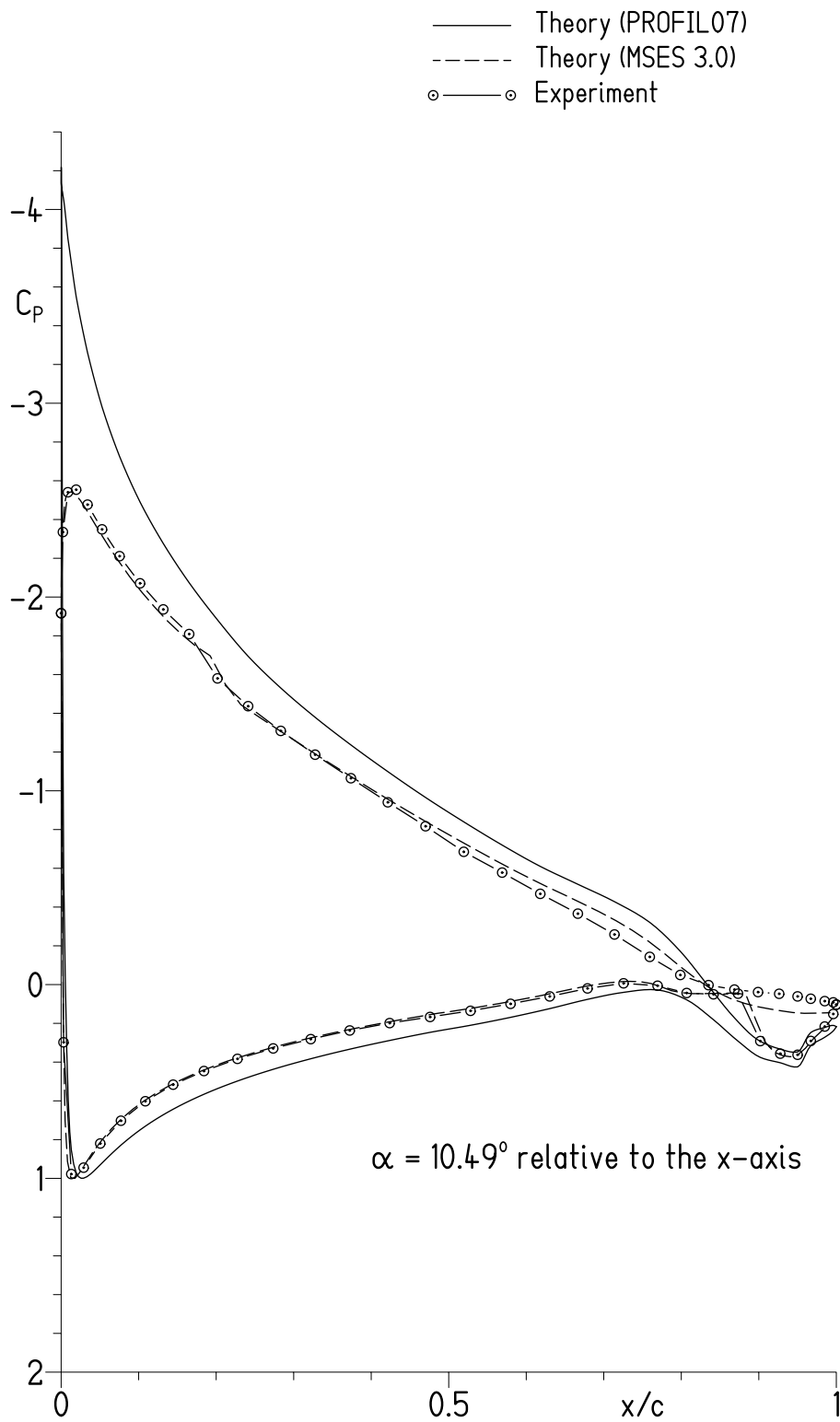
(c) $c_l = 1.14$.

Figure 14.- Concluded.

(a) $R = 0.50 \times 10^6$.

Figure 15.- Comparison of theoretical and experimental section characteristics with transition free.

(b) $R = 0.70 \times 10^6$.

Figure 15.- Continued.

Theory (PROFIL07)
Theory (MSES 3.0)
⊙ Experiment

c_ℓ

2

1.5

c_ℓ

1

0.5

0

5   15 $10^3 c_d$ 20

c_ℓ

2

1.5

1

$c_\ell(\alpha)$

S.U.

c_m
−0.1

T.U.

−0.05

S.L.

−5 $c_m(\alpha)$ 5 α° 10

0.5   x/c   1

0.05

−0.5

−0.5
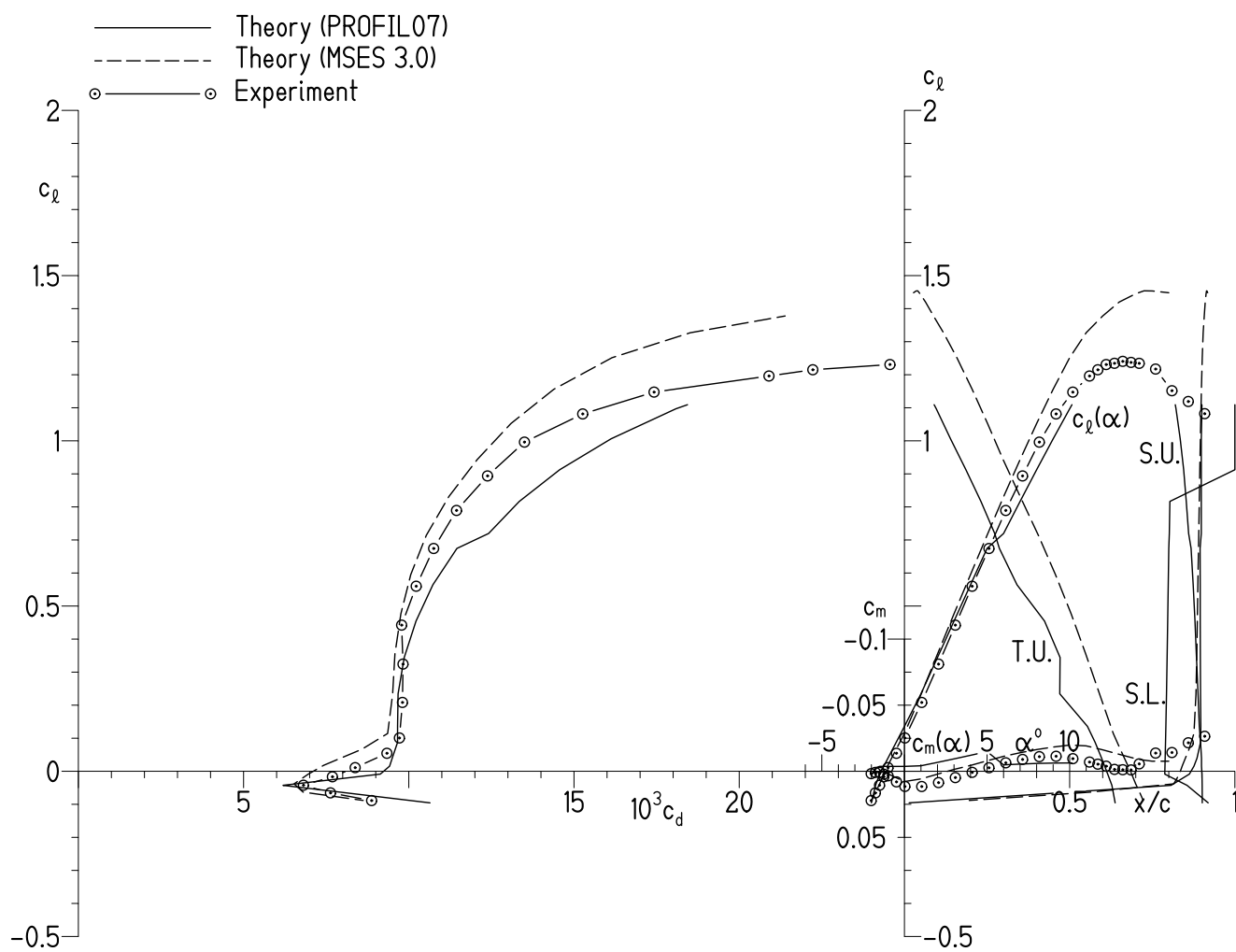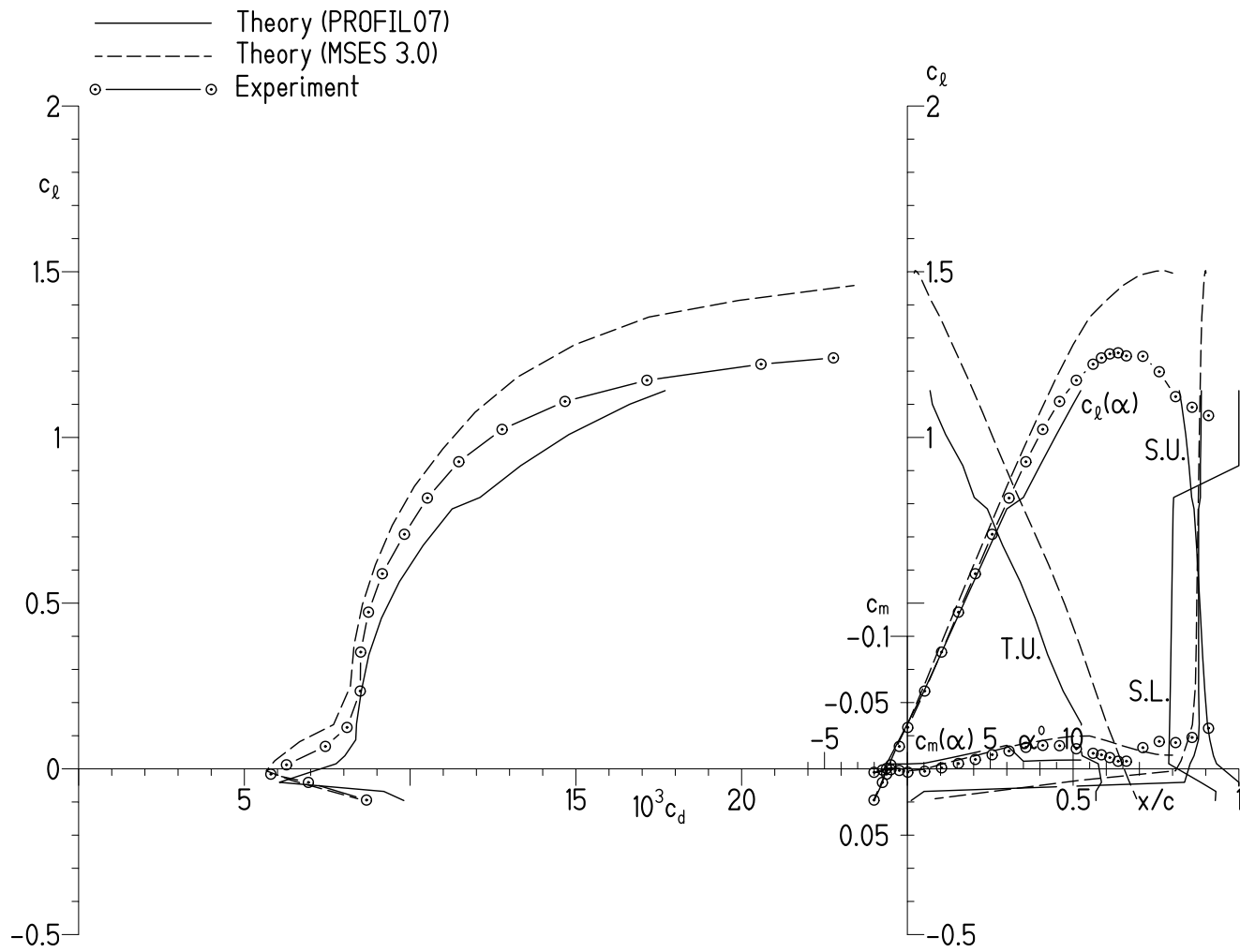
(c) R = 1.00×10^6.

Figure 15.- Continued.

49
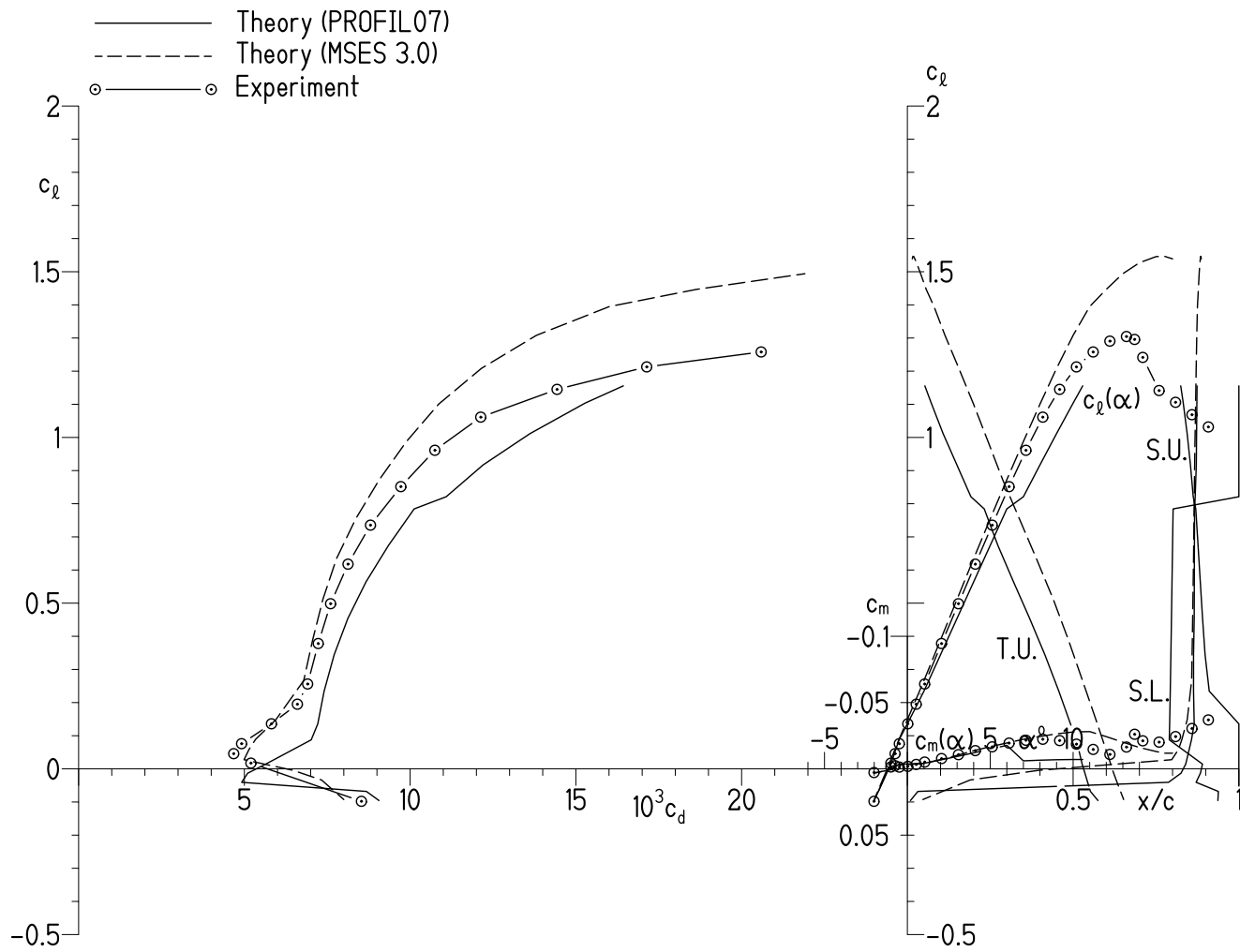
(d) R $= 1.50 \times 10^6$.

Figure 15.- Concluded.
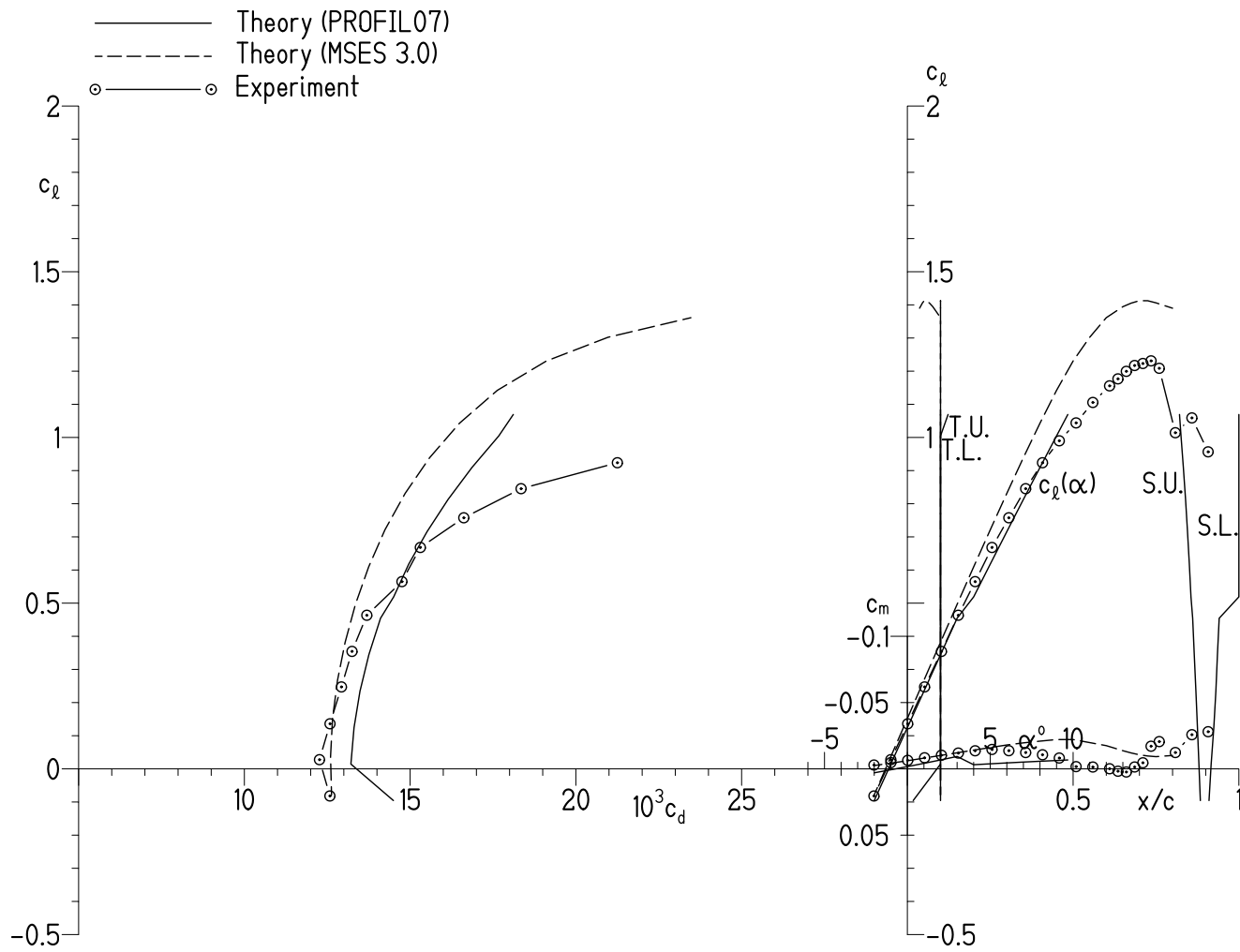
(a) $R = 0.50 \times 10^6$.

Figure 16.- Comparison of theoretical and experimental section characteristics with transition fixed at 0.10c U. and 0.10c L.
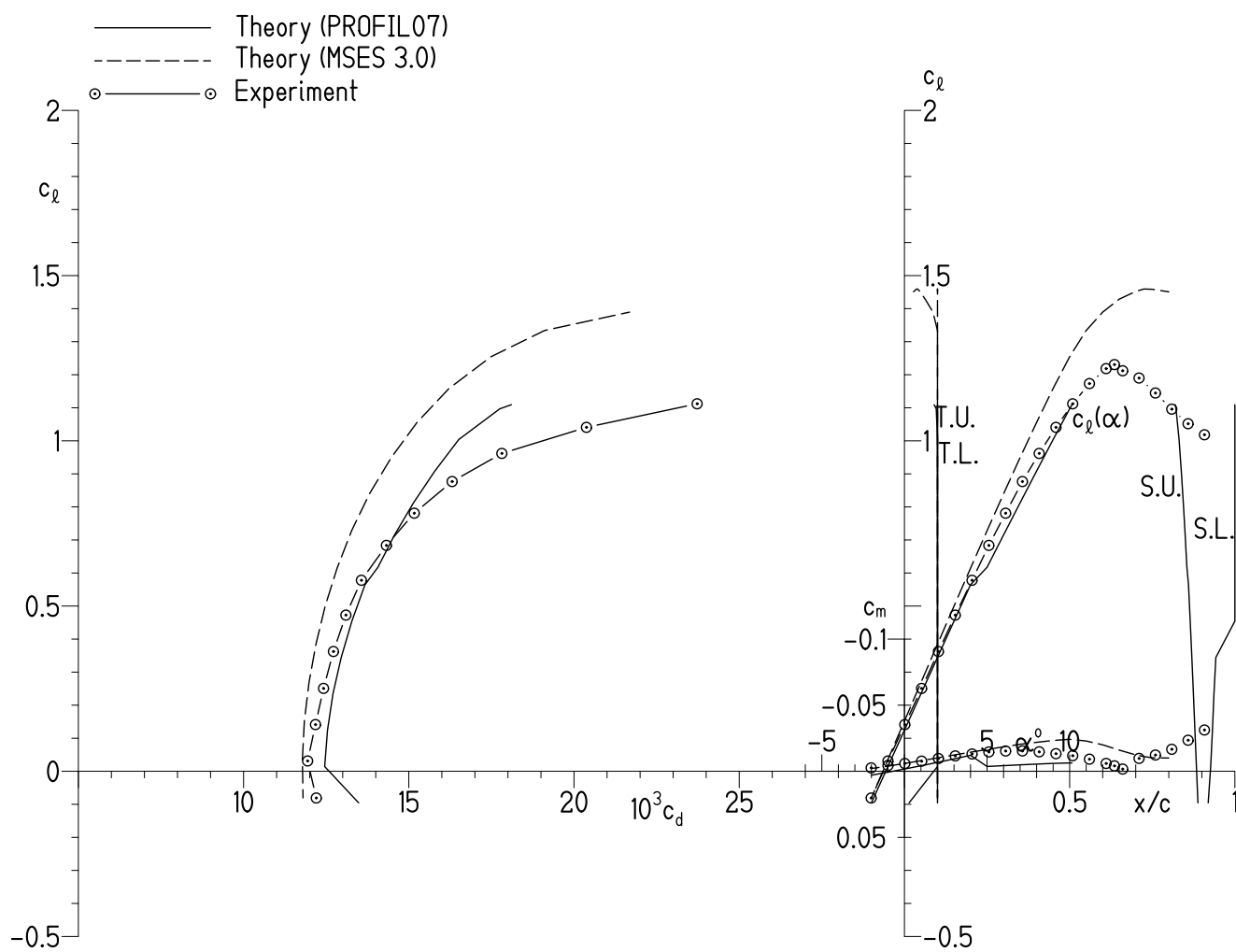
(b) $R = 0.70 \times 10^6$.

Figure 16.- Continued.
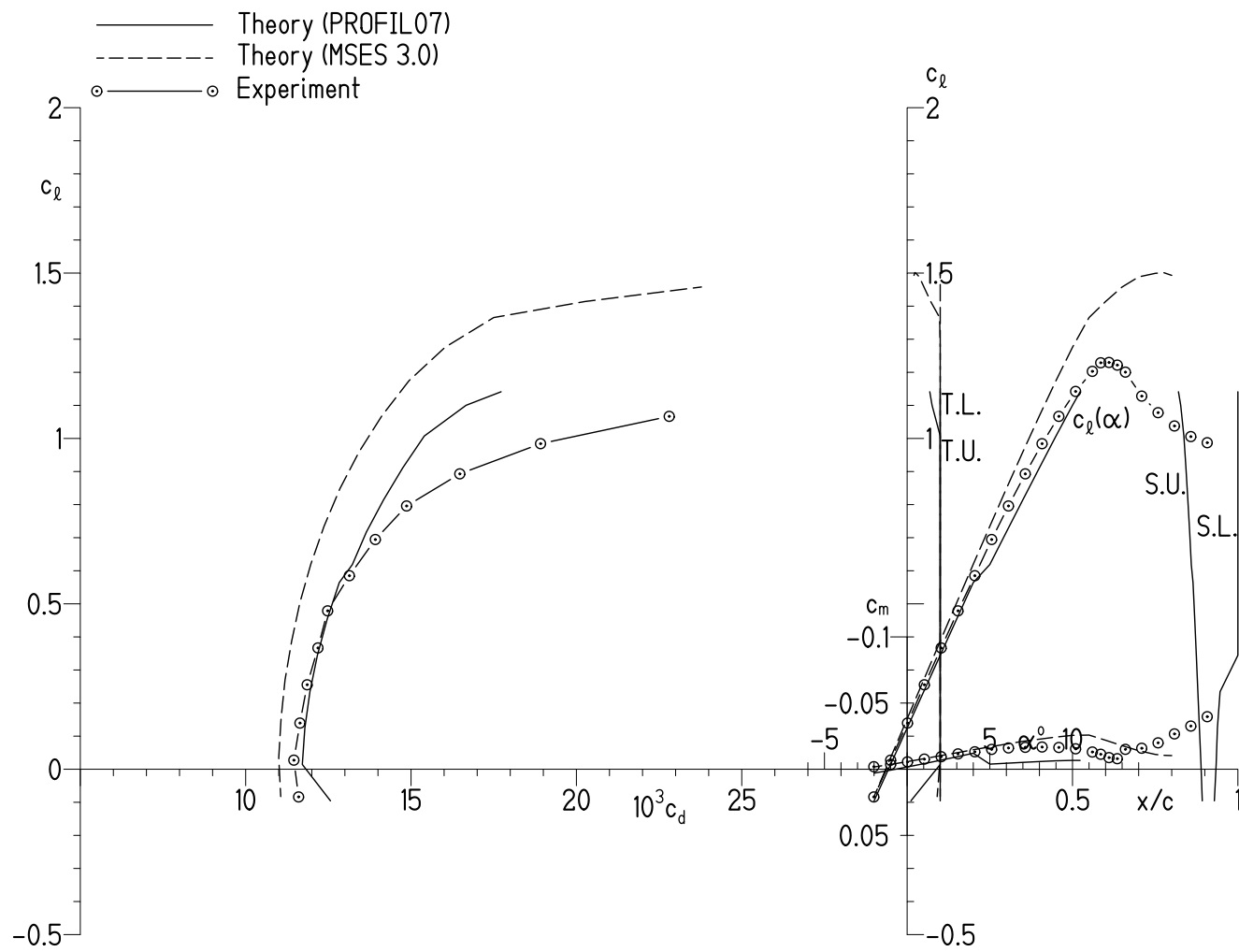
(c) $R = 1.00 \times 10^6$.

Figure 16.- Continued.
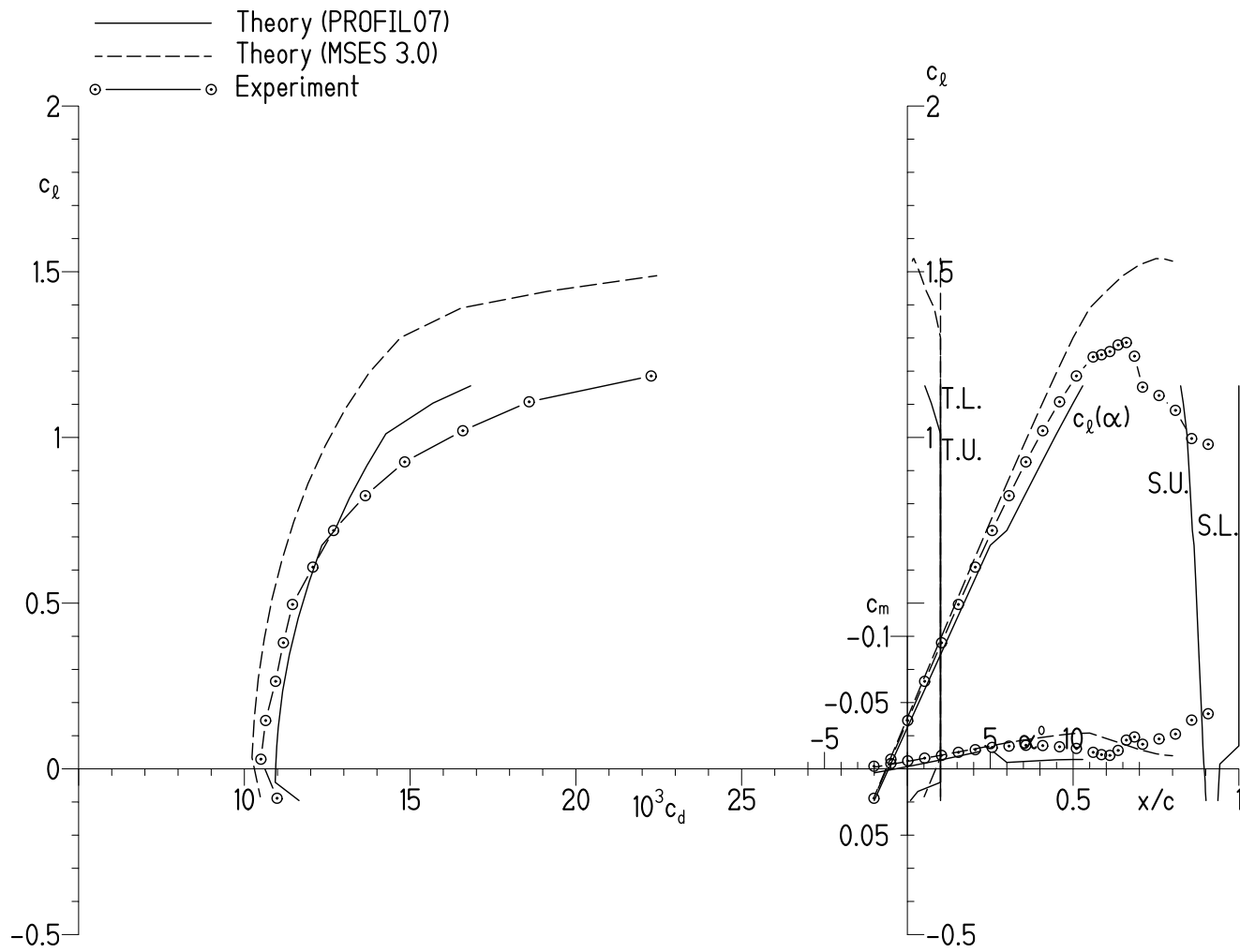
(d) $R = 1.50 \times 10^6$.

Figure 16.- Concluded.
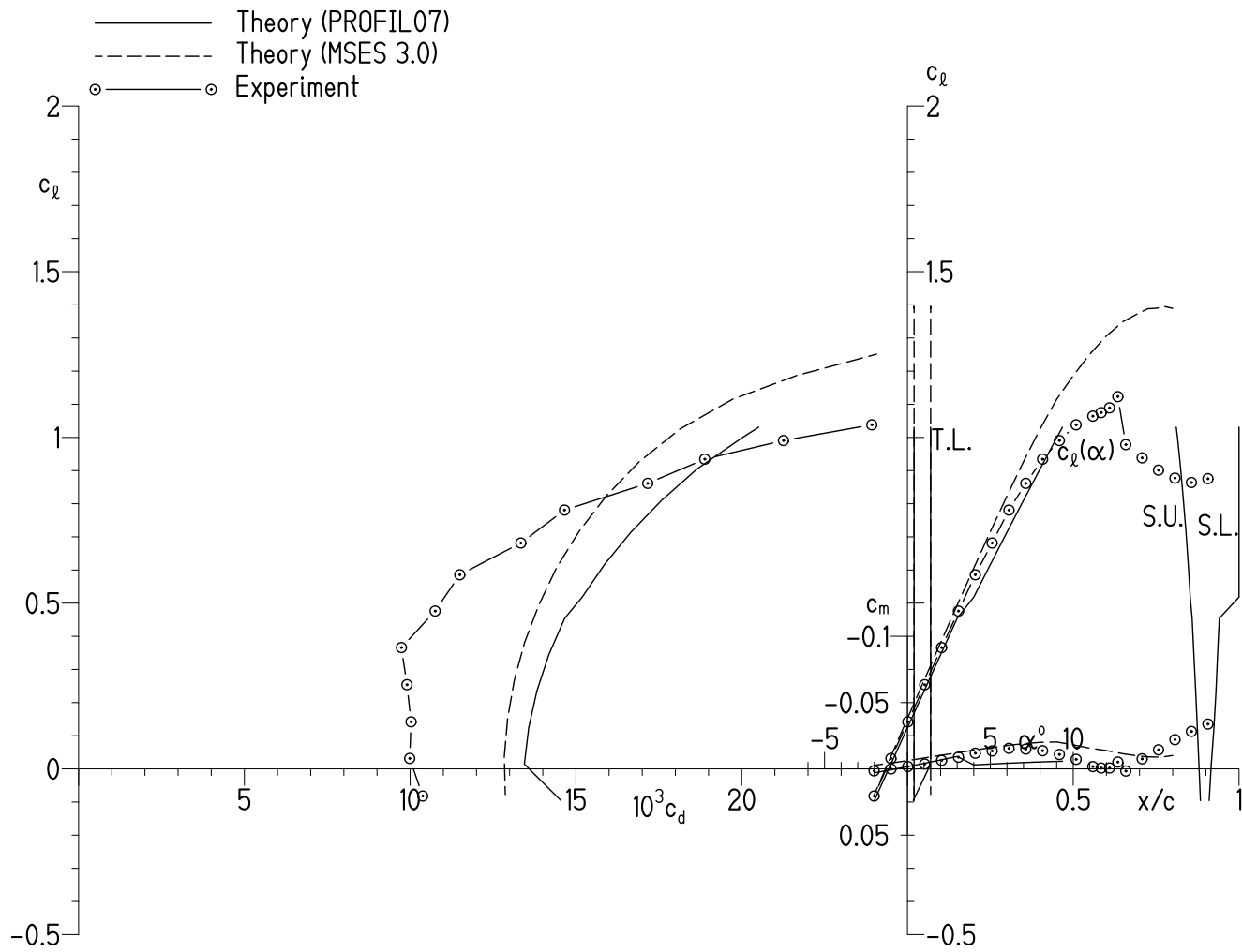
(a) $R = 0.50 \times 10^6$.

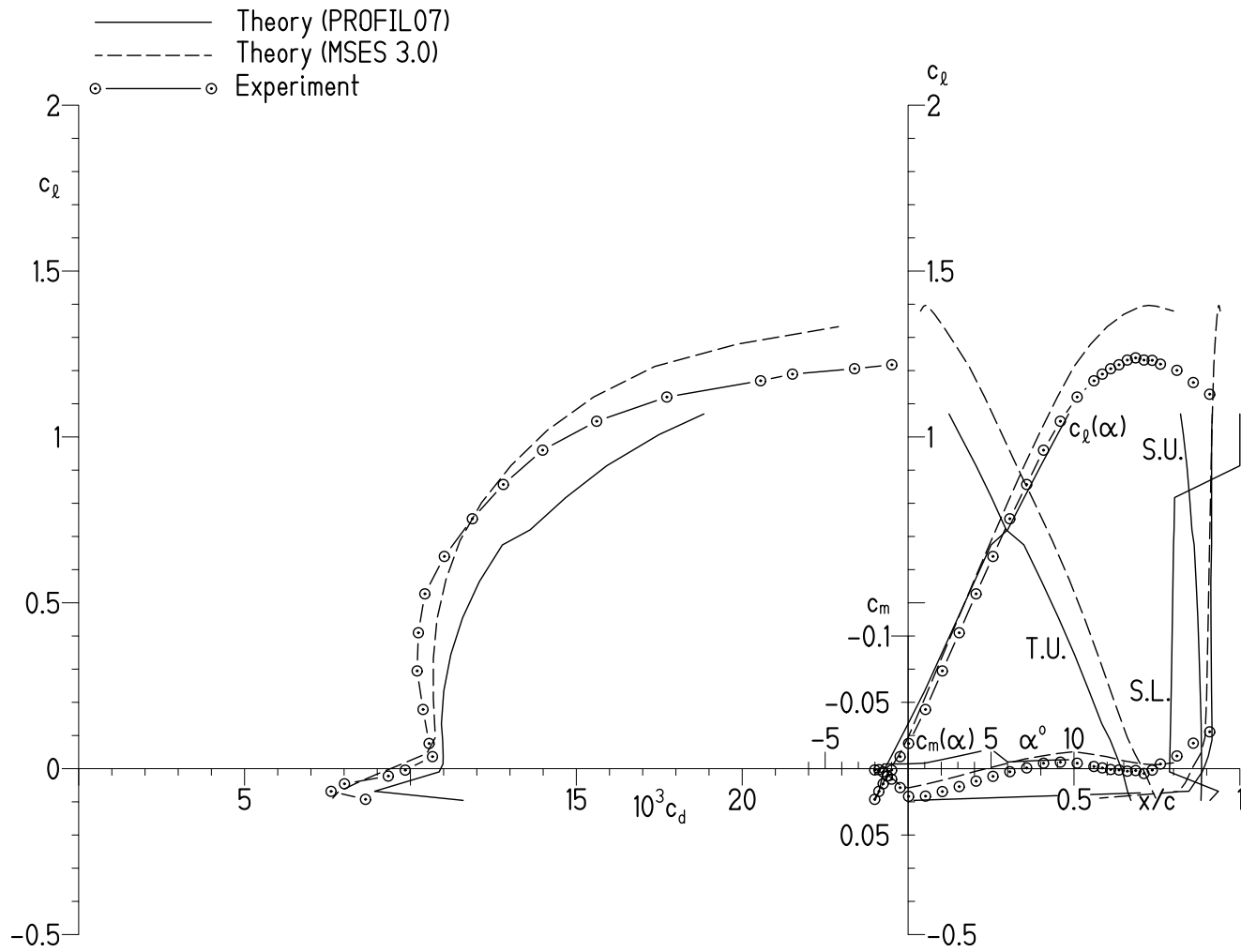Figure 17.- Comparison of theoretical and experimental section characteristics with transition fixed at 0.02c U. and 0.07c L.
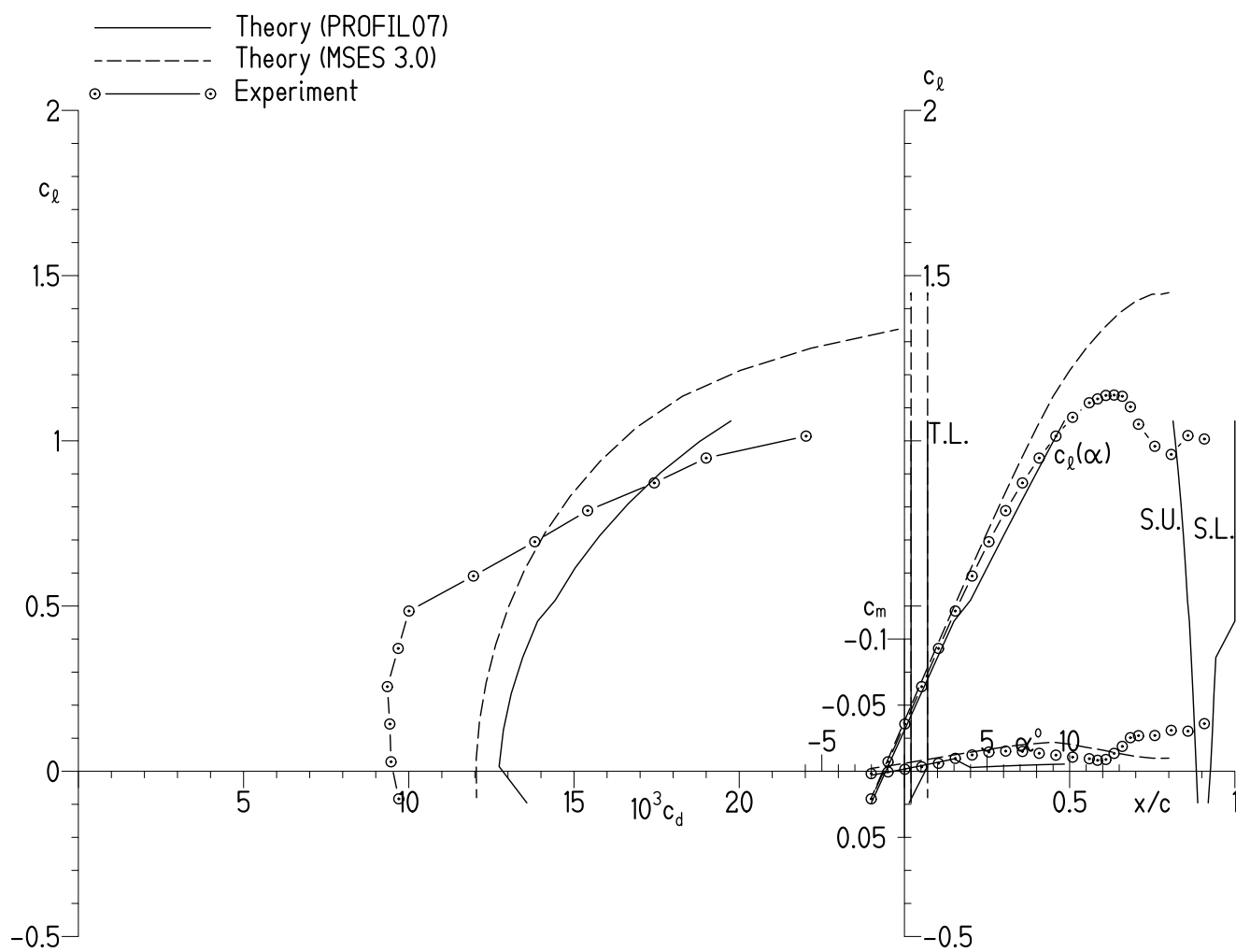
(b) $R = 0.70 \times 10^6$.

Figure 17.- Continued.
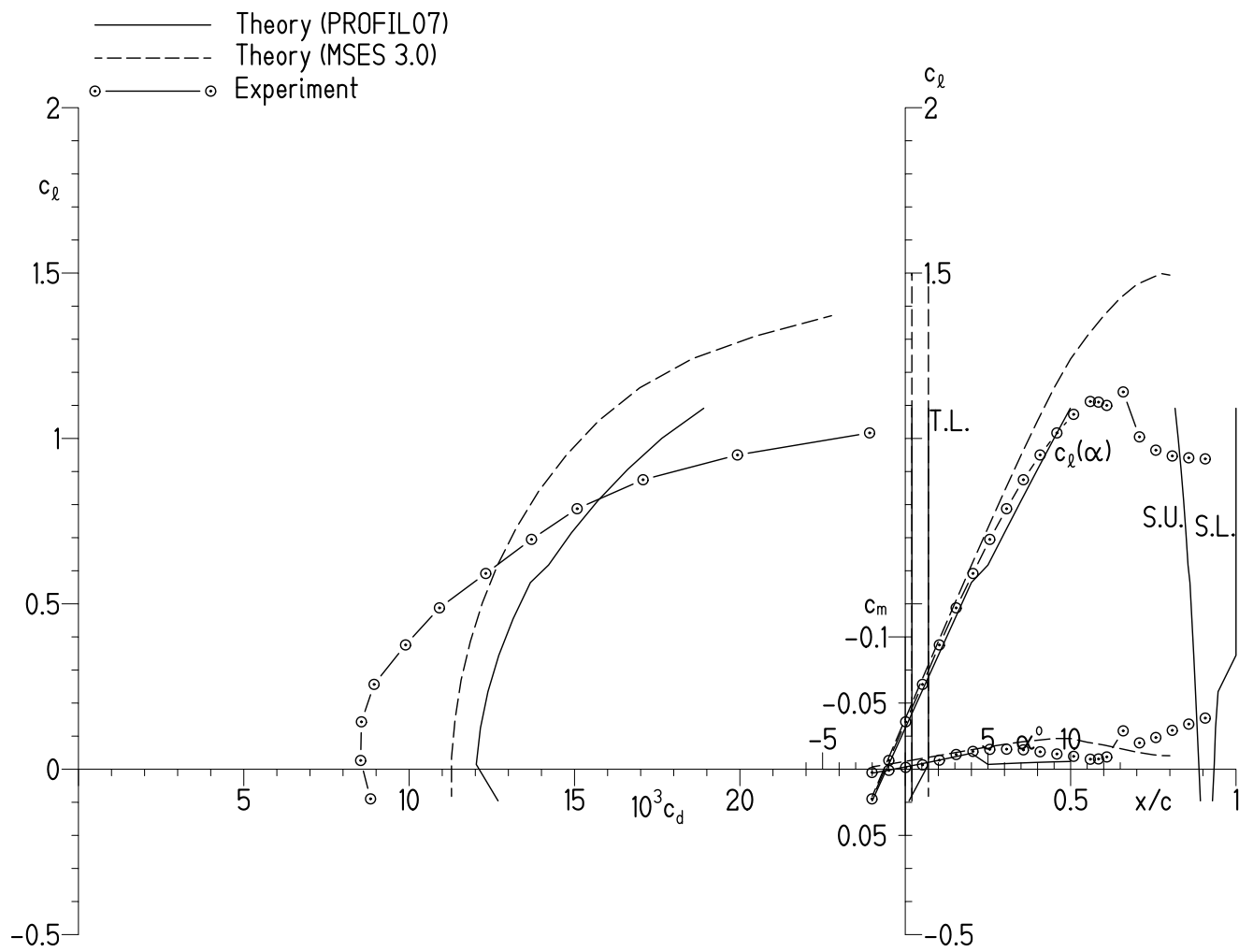
(c) $R = 1.00 \times 10^6$.

Figure 17.- Continued.
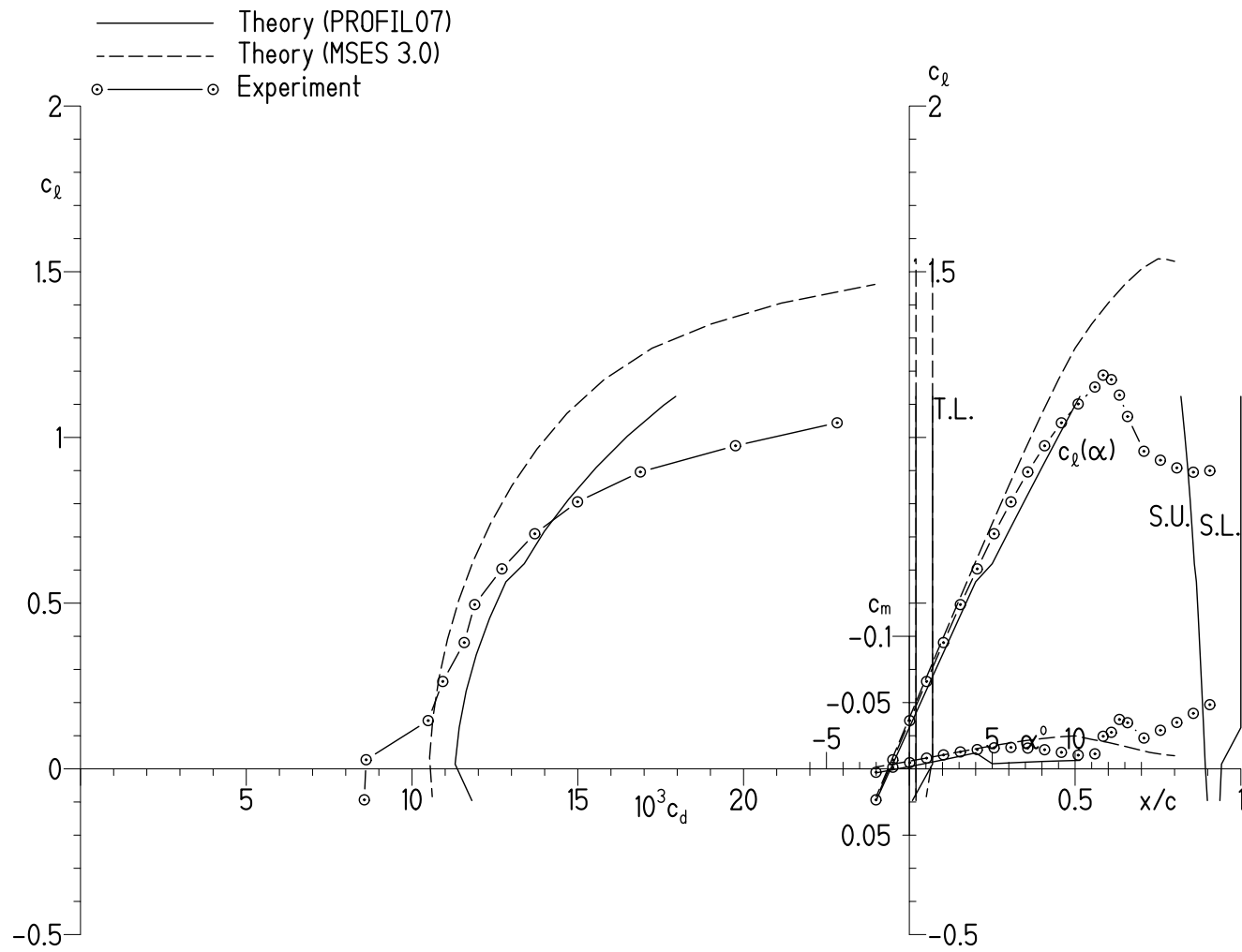
(d) R $= 1.49 \times 10^6$.

Figure 17.- Concluded.
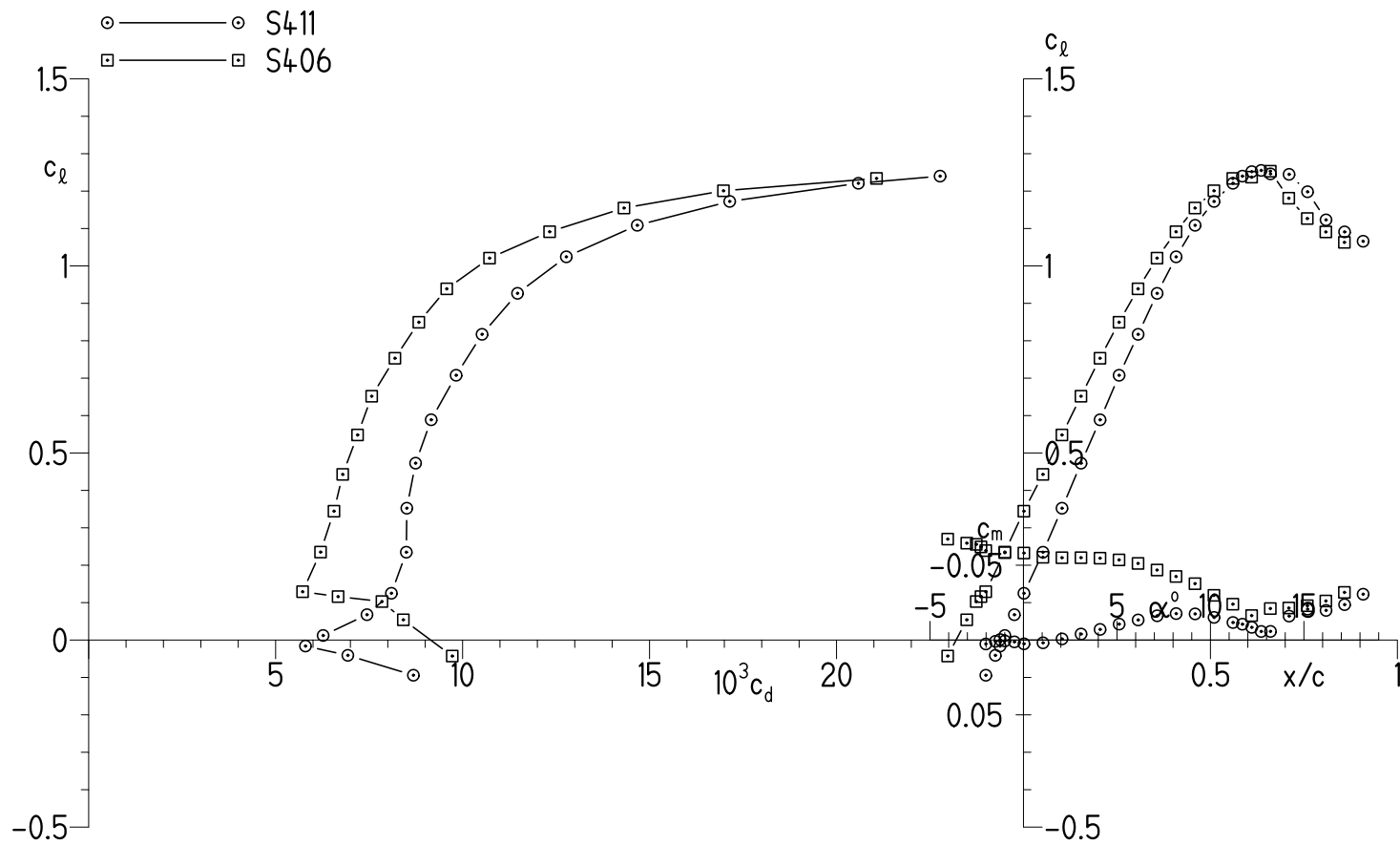
Figure 18.- Comparison of section characteristics of S411 and S406 airfoils for $R = 1.00 \times 10^6$ and $M = 0.1$ with transition free.
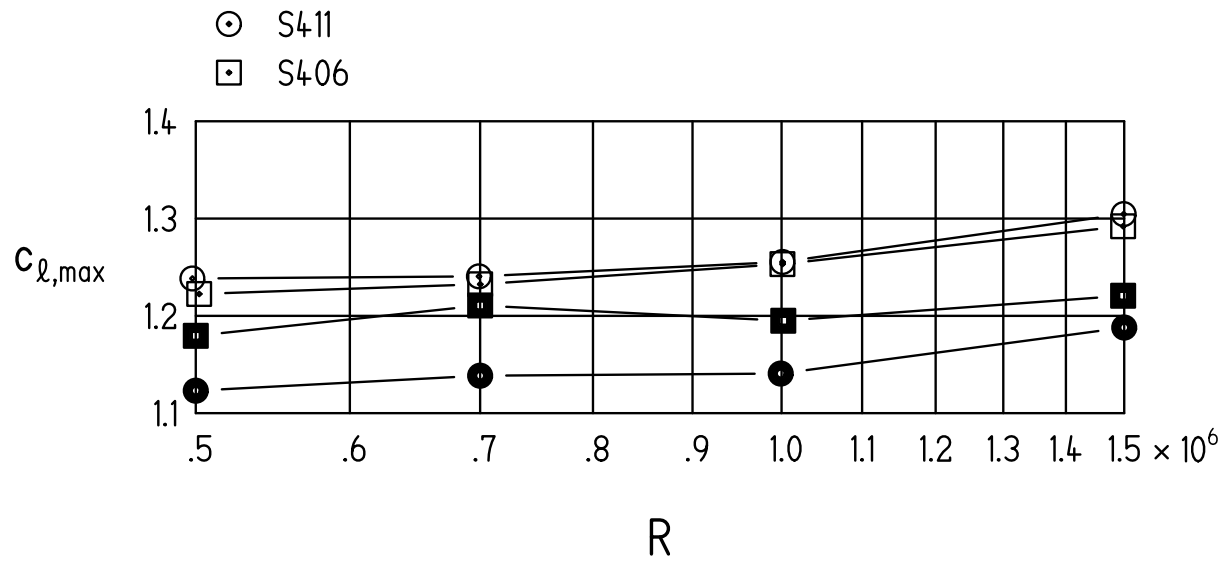
Figure 19.- Comparison of maximum lift coefficients of S411 and S406 airfoils. Open symbols represent data with transition free; solid symbols, data with transition fixed at 0.02c U. and 0.07c L.
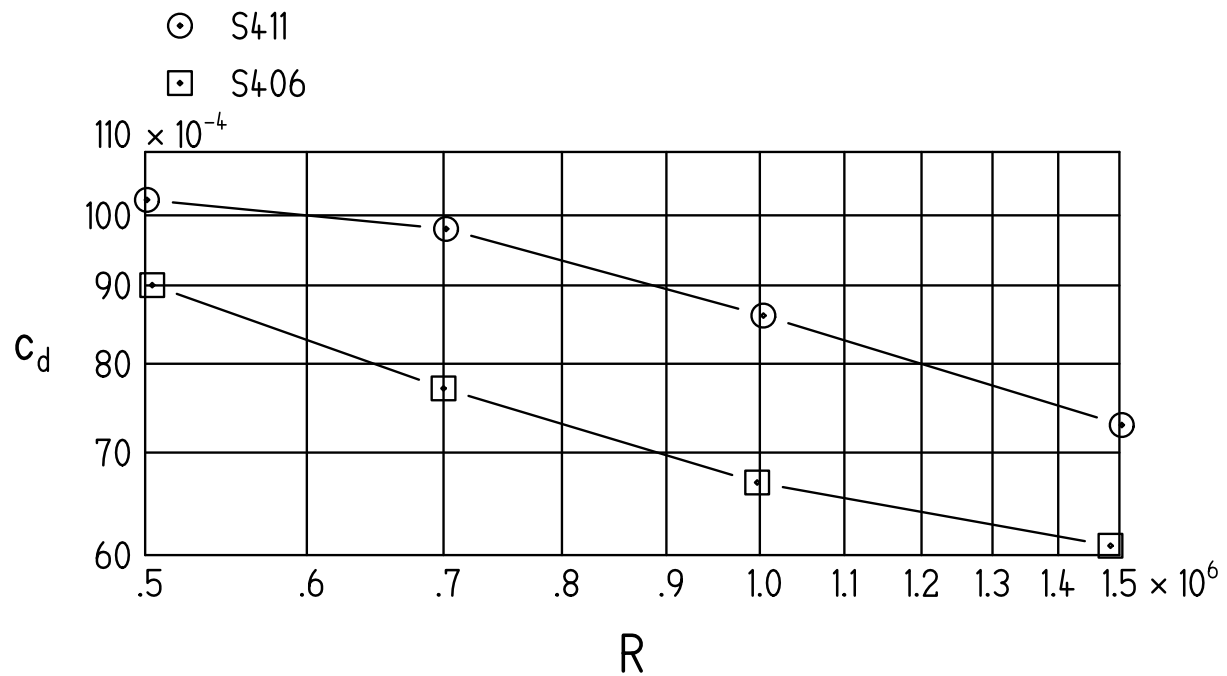
Figure 20.- Comparison of drag coefficients at $c_l = 0.4$ of S411 and S406 airfoils with transition free.

APPENDIX

EXPERIMENTAL SECTION CHARACTERISTICS

$$R = 0.50 \times 10^6, \ M = 0.05, \text{ transition free}$$

α, deg	c_l	c_d	c_m
−2.015	−0.0924	0.008645	0.00093
−1.761	−.0684	.007607	.00071
−1.506	−.0456	.008011	.00242
−1.250	−.0223	.009331	.00540
−.995	−.0043	.009842	.00786
−.484	.0363	.010664	.01426
.027	.0760	.010562	.02083
1.045	.1785	.010379	.02066
2.062	.2947	.010201	.01722
3.079	.4098	.010238	.01347
4.096	.5270	.010434	.00935
5.113	.6398	.011021	.00575
6.130	.7533	.011865	.00226
7.146	.8567	.012799	−.00061
8.161	.9602	.013983	−.00416
9.176	1.0473	.015612	−.00495
10.189	1.1203	.017727	−.00417
11.199	1.1693	.020553	−.00167
11.703	1.1894	.021514	−.00061
12.207	1.2057	.023386	.00061
12.709	1.2176	.024509	.00096
13.212	1.2318	.026975	.00185
13.713	1.2384	.029269	.00137
14.214	1.2319	.032448	.00358
14.712	1.2310	.034953	.00106
15.208	1.2195	.033530	−.00355
16.201	1.2009	.074160	−.00961
17.188	1.1641	.094403	−.01924
18.177	1.1288	.116358	−.02781

R = 0.50 × 10^6, M = 0.05, transition fixed at 0.10c U. and 0.10c L.

α, deg	c_l	c_d	c_m
−2.016	−0.0818	0.012580	−0.00291
−.999	.0277	.012266	−.00472
.019	.1360	.012584	−.00643
1.037	.2472	.012928	−.00837
2.054	.3544	.013247	−.01030
3.071	.4635	.013694	−.01193
4.087	.5650	.014753	−.01365
5.104	.6680	.015308	−.01465
6.120	.7576	.016619	−.01372
7.136	.8454	.018347	−.01232
8.151	.9237	.021252	−.01064
9.164	.9899	.026320	−.00819
10.178	1.0439	.033559	−.00170
11.189	1.1056	.040982	−.00141
12.198	1.1557	.045237	−.00010
12.703	1.1768	.045267	.00176
13.208	1.1995	.042517	.00234
13.708	1.2171	.045800	−.00144
14.207	1.2232	.053339	−.00460
14.701	1.2311	.067949	−.01710
15.194	1.2087	.109979	−.02058
16.165	1.0143	.143099	−.01234
17.165	1.0590	.175851	−.02579
18.144	.9566	.208235	−.02805

R = 0.50 × 10^6, M = 0.05, transition fixed at 0.02c U. and 0.07c L.

α, deg	c_l	c_d	c_m
−2.013	−0.0819	0.010379	0.00148
−.995	.0315	.009986	.00003
.023	.1419	.010027	−.00179
1.041	.2539	.009903	−.00366
2.058	.3660	.009736	−.00640
3.075	.4761	.010753	−.00883
4.092	.5857	.011497	−.01184
5.107	.6815	.013339	−.01354
6.123	.7808	.014655	−.01549
7.137	.8615	.017165	−.01493
8.151	.9345	.018885	−.01369
9.162	.9907	.021260	−.01088
10.173	1.0381	.023925	−.00720
11.181	1.0643	.028751	−.00174
11.684	1.0750	.032530	−.00066
12.186	1.0892	.036644	−.00069
12.689	1.1231	.035622	−.00515
13.168	.9784	.110537	.00162
14.155	.9385	.143651	−.00760
15.143	.9014	.176397	−.01439
16.134	.8772	.208774	−.02204
17.127	.8640	.240783	−.02824
18.124	.8756	.272424	−.03383

$$R = 0.70 \times 10^6, \ M = 0.07, \text{ transition free}$$

α, deg	c_l	c_d	c_m
−2.014	−0.0887	0.008875	0.00179
−1.761	−.0654	.007630	.00084
−1.507	−.0422	.006811	.00079
−1.251	−.0167	.007688	.00219
−.996	.0110	.008377	.00340
−.485	.0544	.009338	.00799
.025	.1008	.009716	.01144
1.044	.2083	.009808	.01151
2.061	.3244	.009825	.00855
3.079	.4423	.009783	.00477
4.096	.5600	.010224	.00080
5.114	.6742	.010752	−.00268
6.131	.7893	.011444	−.00642
7.147	.8938	.012382	−.00899
8.163	.9961	.013500	−.01108
9.177	1.0814	.015263	−.01138
10.190	1.1475	.017422	−.00955
11.200	1.1962	.020900	−.00699
11.705	1.2151	.022227	−.00540
12.208	1.2309	.024561	−.00389
12.711	1.2347	.028408	−.00145
13.212	1.2406	.033571	−.00119
13.712	1.2374	.037884	−.00104
14.208	1.2346	.041845	−.00563
15.200	1.2173	.060344	−.01378
16.189	1.1517	.069930	−.01420
17.179	1.1191	.087597	−.02157
18.170	1.0823	.107057	−.02651

$R = 0.70 \times 10^6$, $M = 0.07$, transition fixed at 0.10c U. and 0.10c L.

α, deg	c_l	c_d	c_m
−2.016	−0.0809	0.012200	−0.00259
−.998	.0312	.011938	−.00439
.020	.1413	.012176	−.00588
1.038	.2508	.012420	−.00769
2.055	.3624	.012719	−.00968
3.073	.4726	.013096	−.01164
4.090	.5780	.013565	−.01308
5.107	.6836	.014322	−.01465
6.123	.7810	.015165	−.01535
7.140	.8768	.016311	−.01542
8.155	.9619	.017816	−.01475
9.169	1.0408	.020376	−.01334
10.183	1.1121	.023726	−.01181
11.195	1.1733	.026440	−.00918
12.205	1.2186	.026957	−.00594
12.708	1.2308	.029533	−.00411
13.207	1.2121	.041927	−.00168
14.198	1.1901	.047773	−.00977
15.189	1.1448	.062063	−.01232
16.178	1.0960	.076220	−.01667
17.166	1.0518	.096887	−.02351
18.156	1.0184	.114726	−.03124

R = 0.70 × 10^6, M = 0.07, transition fixed at 0.02c U. and 0.07c L.

α, deg	c_l	c_d	c_m
−2.013	−0.0835	0.009697	0.00177
−.995	.0287	.009462	.00048
.023	.1430	.009425	−.00152
1.042	.2561	.009351	−.00336
2.059	.3717	.009679	−.00604
3.076	.4849	.010005	−.00977
4.093	.5909	.011955	−.01234
5.109	.6946	.013812	−.01457
6.125	.7887	.015411	−.01529
7.139	.8727	.017428	−.01499
8.153	.9479	.018999	−.01360
9.165	1.0143	.022022	−.01221
10.176	1.0712	.025955	−.01070
11.185	1.1152	.033921	−.00951
11.688	1.1269	.039670	−.00834
12.189	1.1374	.038407	−.00894
12.687	1.1385	.052147	−.01354
13.182	1.1348	.050808	−.01886
13.673	1.1029	.062201	−.02541
14.163	1.0502	.066024	−.02693
15.151	.9835	.077905	−.02707
16.145	.9589	.092281	−.03099
17.156	1.0160	.109349	−.03038
18.150	1.0056	.126185	−.03604

$$R = 1.00 \times 10^6, \quad M = 0.10, \text{ transition free}$$

α, deg	c_l	c_d	c_m
−2.014	−0.0941	0.008684	0.00259
−1.506	−.0409	.006931	.00083
−1.253	−.0160	.005798	−.00034
−.998	.0122	.006270	.00055
−.488	.0678	.007443	.00118
.023	.1250	.008096	.00249
1.042	.2348	.008495	.00181
2.060	.3524	.008508	−.00079
3.078	.4728	.008743	−.00406
4.096	.5888	.009160	−.00713
5.114	.7078	.009827	−.01069
6.131	.8172	.010520	−.01347
7.148	.9268	.011469	−.01626
8.164	1.0244	.012774	−.01772
9.178	1.1087	.014671	−.01752
10.191	1.1725	.017143	−.01518
11.202	1.2210	.020584	−.01177
11.706	1.2401	.022769	−.01063
12.209	1.2521	.025200	−.00854
12.712	1.2554	.030068	−.00578
13.210	1.2462	.033064	−.00582
14.204	1.2449	.047024	−.01605
15.193	1.1984	.064442	−.02072
16.181	1.1232	.072279	−.01985
17.173	1.0911	.091431	−.02372
18.165	1.0661	.111591	−.03067

R = 1.00×10^6, M = 0.10, transition fixed at 0.10c U. and 0.10c L.

α, deg	c_l	c_d	c_m
−2.016	−0.0838	0.011600	−0.00194
−.998	.0274	.011457	−.00368
.020	.1395	.011641	−.00558
1.039	.2553	.011859	−.00766
2.056	.3667	.012185	−.00947
3.074	.4788	.012478	−.01160
4.091	.5851	.013135	−.01318
5.109	.6945	.013920	−.01500
6.126	.7959	.014865	−.01611
7.142	.8930	.016474	−.01656
8.158	.9842	.018916	−.01680
9.172	1.0668	.022806	−.01645
10.186	1.1422	.026255	−.01544
11.198	1.2029	.028282	−.01302
11.704	1.2288	.026688	−.01133
12.206	1.2298	.032058	−.00879
12.705	1.2218	.043685	−.00798
13.197	1.2006	.037393	−.01504
14.184	1.1281	.048878	−.01587
15.173	1.0780	.062920	−.01995
16.162	1.0378	.082900	−.02672
17.153	1.0057	.102282	−.03264
18.145	.9872	.123242	−.03972

$R = 1.00 \times 10^6$, $M = 0.10$, transition fixed at 0.02c U. and 0.07c L.

α, deg	c_l	c_d	c_m
−2.014	−0.0897	0.008832	0.00246
−.995	.0265	.008533	.00082
.024	.1433	.008556	−.00138
1.042	.2565	.008939	−.00331
2.060	.3758	.009891	−.00688
3.076	.4878	.010915	−.01114
4.092	.5918	.012316	−.01347
5.109	.6949	.013698	−.01501
6.125	.7876	.015078	−.01517
7.140	.8752	.017071	−.01466
8.154	.9501	.019925	−.01320
9.167	1.0168	.023921	−.01151
10.178	1.0729	.028769	−.00976
11.186	1.1118	.038647	−.00758
11.685	1.1099	.063747	−.00777
12.183	1.1000	.033578	−.00929
13.177	1.1407	.058448	−.02902
14.160	1.0048	.060462	−.01993
15.151	.9646	.077594	−.02398
16.144	.9471	.093938	−.02941
17.141	.9415	.110688	−.03413
18.137	.9383	.126195	−.03867

$$R = 1.50 \times 10^6, \ M = 0.16, \text{ transition free}$$

α, deg	c_l	c_d	c_m
−2.015	−0.0979	0.008531	0.00275
−.998	.0173	.005197	−.00144
−.744	.0458	.004678	−.00241
−.488	.0760	.004916	−.00135
.022	.1360	.005817	−.00190
.531	.1951	.006599	−.00338
1.041	.2561	.006908	−.00515
2.060	.3782	.007228	−.00780
3.079	.4983	.007601	−.01074
4.097	.6177	.008126	−.01378
5.116	.7354	.008804	−.01664
6.134	.8516	.009720	−.01947
7.151	.9613	.010746	−.02161
8.168	1.0613	.012130	−.02238
9.184	1.1451	.014432	−.02136
10.197	1.2129	.017137	−.01866
11.207	1.2580	.020589	−.01470
12.216	1.2907	.026147	−.01092
13.215	1.3046	.025493	−.01649
13.707	1.2958	.026092	−.02614
14.201	1.2416	.051336	−.02119
15.185	1.1416	.060680	−.02021
16.177	1.1061	.081974	−.02438
17.167	1.0687	.100263	−.03048
18.156	1.0318	.120022	−.03695

R = 1.50×10^6, M = 0.16, transition fixed at 0.10c U. and 0.10c L.

α, deg	c_l	c_d	c_m
−2.017	−0.0887	0.010986	−0.00201
−.998	.0291	.010498	−.00407
.021	.1459	.010642	−.00608
1.040	.2641	.010941	−.00812
2.059	.3806	.011176	−.01019
3.077	.4961	.011451	−.01249
4.095	.6087	.012065	−.01448
5.113	.7192	.012690	−.01621
6.131	.8243	.013649	−.01717
7.148	.9262	.014835	−.01780
8.164	1.0203	.016589	−.01760
9.180	1.1076	.018590	−.01668
10.195	1.1855	.022271	−.01542
11.207	1.2428	.025327	−.01250
11.709	1.2495	.030503	−.01075
12.212	1.2592	.031791	−.01019
12.712	1.2791	.026072	−.01393
13.208	1.2864	.025554	−.02171
13.700	1.2452	.033827	−.02410
14.188	1.1518	.048864	−.01860
15.181	1.1266	.066516	−.02261
16.171	1.0818	.084674	−.02628
17.149	.9967	.098127	−.03681
18.144	.9794	.119014	−.04161

$R = 1.49 \times 10^6$, $M = 0.16$, transition fixed at 0.02c U. and 0.07c L.

α, deg	c_l	c_d	c_m
−2.014	−0.0934	0.008560	0.00255
−.996	.0275	.008615	−.00126
.022	.1456	.010486	−.00468
1.040	.2636	.010927	−.00812
2.059	.3811	.011574	−.01055
3.077	.4956	.011889	−.01279
4.094	.6034	.012711	−.01456
5.112	.7094	.013702	−.01588
6.128	.8057	.014992	−.01621
7.144	.8959	.016886	−.01569
8.159	.9750	.019756	−.01444
9.172	1.0442	.022822	−.01249
10.184	1.1011	.027493	−.01037
11.192	1.1521	.028354	−.01135
11.689	1.1880	.022204	−.02462
12.185	1.1746	.022540	−.02760
12.671	1.1278	.029760	−.03730
13.161	1.0632	.067349	−.03484
14.151	.9584	.069024	−.02326
15.143	.9314	.087312	−.02911
16.135	.9082	.106581	−.03504
17.129	.8952	.124947	−.04188
18.125	.8998	.143684	−.04844

REPORT DOCUMENTATION PAGE

Form Approved
OMB No. 0704-0188

1. REPORT DATE *(DD-MM-YYYY)*	**2. REPORT TYPE**	**3. DATES COVERED** *(From - To)*
xx 08 2010	FINAL REPORT	Sep 2007 Jun 2010

4. TITLE AND SUBTITLE

Design and Experimental Results for the S411 Airfoil

5a. CONTRACT NUMBER
W911W6 07 C 0047

5b. GRANT NUMBER

5c. PROGRAM ELEMENT NUMBER

6. AUTHOR(S)

Somers, Dan M. and Maughmer, Mark D.

5d. PROJECT NUMBER

5e. TASK NUMBER

5f. WORK UNIT NUMBER

7. PERFORMING ORGANIZATION NAME(S) AND ADDRESS(ES)

Airfoils, Incorporated
Attn: Dan M. Somers
122 Rose Drive
Port Matilda PA 16870 7535

8. PERFORMING ORGANIZATION REPORT NUMBER

SBIR Topic Number A06 006
Proposal Number A2 2972

9. SPONSORING / MONITORING AGENCY NAME(S) AND ADDRESS(ES)

US Army Aviation Research, Development and Engineering
  Command (RDECOM)
Aviation Applied Technology Directorate (AATD)
Fort Eustis VA 23604 5577

10. SPONSOR/MONITOR'S ACRONYM(S)

11. SPONSOR/MONITOR'S REPORT NUMBER(S)
RDECOM TR 10 D 111

12. DISTRIBUTION / AVAILABILITY STATEMENT

Approved for public release; distribution is unlimited.

13. SUPPLEMENTARY NOTES

UL Note: No proprietary / limited information may be included in the abstract.

14. ABSTRACT

A 14 percent thick airfoil, the S411, intended for rotorcraft applications has been designed and analyzed theoretically and verified experimentally in The Pennsylvania State University Low Speed, Low Turbulence Wind Tunnel. The airfoil incorporates a 5 percent chord tab. The two primary objectives of high maximum lift and low profile drag have been achieved. The constraint on the pitching moment has been exceeded; that on the airfoil thickness, satisfied. The airfoil exhibits a docile stall. Comparisons of the theoretical and experimental results generally show good agreement. Comparisons with the S406 airfoil confirm the achievement of the objectives.

15. SUBJECT TERMS

Airfoils, rotorcraft, laminar flow, wind tunnel

16. SECURITY CLASSIFICATION OF:			**17. LIMITATION OF ABSTRACT**	**18. NUMBER OF PAGES**	**19a. NAME OF RESPONSIBLE PERSON** Dan M. Somers
a. REPORT unclassified	**b. ABSTRACT** unclassified	**c. THIS PAGE** unclassified	UU	73	**19b. TELEPHONE NUMBER** *(include area code)* (814) 357 0500

Standard Form 298 (Rev. 8-98)
Prescribed by ANSI Std. Z39.18